Optimization of Steel Production: Ladle Furnace Slag and Caster Productivity

By

Kailash Bathy Vodeyar Math

Department of Mechanical Engineering

McGill University

Montreal, Canada

December 2012

A thesis submitted to McGill University in partial fulfillment of the requirement for the degree of Master of Engineering

Abstract

A slag optimization model is the first objective of this thesis. The importance of slag has been very well understood by the steelmaking industry to produce cost effective, quality steel, where the slag phase has become an essential part of steel making process. The composition and properties of slag play an important role in protecting furnace refractories. The research focused on the development of a slag model to have optimum slag saturated with MgO for better refractory life. A computer model was developed to calculate minimum MgO required during the ladle refining process. The effect of the desulfurization process on optical basicity and MgO requirement is discussed. The plant data at Arcelormittal Contrecoeur West were used to compare the results generated by the model for usage of MgO and CaO. The application of the slag model at the ladle metallurgical facility can increase the life of the refractory and can result in reduced usage of additives to generate sufficient MgO and CaO.

The second objective of the thesis is to increase the casting throughput of a continuous caster to improve the factory throughput. An experimental investigation of heat flow during the production of steel billets was undertaken. This research measured the cooling rate of the molten steel at the casting facility by systematic measurement of the steel temperature at several points during the casting process by the use of a pyrometer. A 2D steady state heat transfer simulation model was developed to produce data on temperature and phase distributions for different casting rates. The model data for billet surface temperatures were compared to measured surface temperatures. The comparison between measured and calculated surface temperatures was reasonable and the two sets of data were within ± 30-40 °C. The model data can be used to predict optimum casting speed based on the liquid well closure position and its corresponding surface temperature. This predicted parameter can be monitored by using sensors, and the casting rate can be controlled through a feedback system.

Résumé

Un modèle d'optimisation de laitier est le premier objectif de cette thèse. L'importance de laitier dans la qualité et la rentabilité de l'acier a été très bien comprise par l'industrie sidérurgique. En effet, la phase de laitier est devenue une partie essentielle du processus de production d'acier. La composition et les propriétés du laitier jouent un rôle important dans la protection des réfractaires de four. La recherche s'est portée sur le développement d'un modèle de laitier afin d'avoir le laitier optimal, saturé en MgO, pour allonger la vie de réfractaire. Un modèle informatique a été développé pour calculer la quantité de MgO minimale requise lors du processus de l'affinage en poche. L'effet de la désulfuration sur la basicité optique et l'exigence de MgO est discuté. Les données de l'usine Arcelormittal Contrecoeur-Ouest ont été utilisées pour comparer les résultats générés par le modèle pour l'utilisation de MgO et CaO. L'application du modèle de laitier dans l'installation de métallurgie en poche peut augmenter la durée de vie du réfractaire et peut réduire la quantité d'additifs utilisée pour générer suffisamment de MgO et de CaO.

Le deuxième objectif de la thèse est d'augmenter le débit de coulée d'une machine de coulée continue afin d'améliorer la capacité de production de l'usine. Une étude expérimentale du flux de chaleur lors de la production de billettes d'acier a été entreprise. Cette recherche a mesuré la vitesse de refroidissement de l'acier en fusion dans l'installation de coulée par la mesure systématique de la température de l'acier à travers un pyromètre sur plusieurs points pendant le processus de coulée. Un modèle de simulation à 2D de transfert de chaleur à l'état d'équilibre thermique a été développé pour produire des données sur la répartition de la température de phase à des vitesses de coulée différentes. Les données de modèle concernant la température de surface de la billette a été comparée à la température de surface mesurée. La comparaison entre les températures de surface mesurées et calculées était raisonnable et les deux ensembles de données ont été à l'intérieur de ± 30-40 ° C. Les données modèles peuvent être utilisées pour prédire la vitesse de coulée optimale en fonction de la position de fermeture du puits et sa température de surface correspondante. Ce paramètre prédit peut être suivi en utilisant des capteurs et la vitesse de coulée peut être contrôlée par un système de rétroaction.

Acknowledgement

I would like to gratefully acknowledge the enthusiastic supervision of Professor Vincent Thomson during this work. His invaluable guidance and encouragement during the course of my research work were very helpful.

I would also like to thank Dr. Onur Hisarciklilar for his efforts in development of the slag calculator and for his continuous support and motivation. I further wish to thank Prof. Frank Mucciard, Prof. In-Ho Jung, and Prof. Helmi Attia for their helpful suggestions.

I heartily thank my graduate coordinator Joyce Nault and all the administrative staff for their help.

A special thanks to Mr. Alexandre Rail manager at Arcelormittal for his kind support and guidance towards development of the project. I am indebted to the help and assistance from employees at Arcelormittal: Pascal Gaudreau, Lamanna Mario, Ouellet Réal, Baril Mario and Denis Vaillancourt. A very special thanks to Rob Nunnington retired researcher for his valuable guidance on slag optimization techniques.

I further wish to thank my close friends Mr. Harshad Yadav, Ms. Shalaka and Mr. Amit Tendolkar for believing in me and for their unconditional support and love. I thank all my friends in India for their endless love and encouragement. I also thank my best friends in Montreal, Pratik, Amrut, Kiran, Kaustubha, Senthil, Simarn, Raj, Mirunalini and Pranav for being with me whenever I needed, and for their constant moral support.

I am always thankful to my elder brother, Mr. Karthik for his support and motivation throughout my life.

Finally, I cannot thank enough my mother and father, Mrs. Shambhavi and Mr. Jagadish for believing in me and for their never ending love and support throughout my life and career.

Table of Contents

List of Tables

Part 1- Ladle Furnace Slag Optimization

List of Figures

Part 1 – Ladle Furnace Slag Optimization

Part 2 – Caster Productivity

Chapter 1 Introduction

1.1 Background

The steel industry is one of the most valuable global businesses and is considered as the fundamental material for infrastructure and economic development[1]. Growth in material quality and product development has substantially increased the steel manufacturing potential around the globe. Excellent formability, alloying combinations and crystal arrangements in steel have given an added advantage to the steel industry as well as created new challenges[2].

The long journey from ancient steel manufacturing has seen a tremendous achievement in manufacturing and materials. Carbon steel, high speed steel, low alloy steel and stainless steel are some of the modern steels that have been in development for a long time[3].

The World Steel Association (WSA) has noted that there has been a substantial increase in the demand for steel with crude steel production in 2011 reaching 1,527 megatonnes (Mt), an increase of 6.8% compared to 2010[4]. The WSA also indicated that around 62 countries reported that a total of 136 million tons of steel were manufactured in March 2012. WSA forecasted that steel use would increase by 3.6% in 2012[4].

The steelmaking process has changed over the years. The industrial revolution changed the orthodox way of producing steel into a two category processes: primary and secondary steelmaking, where primary steelmaking uses new iron and secondary steelmaking uses mostly scrap steel as a raw material[5].

1.2 Arcelormittal

Arcelormittal is one of the leading steelmaking companies in the world. Operating in around 60 countries, it is a leader in all the main steel markets. Supplying diverse markets from automotive to construction, Arcelormittal has an annual production of 130 million tons[6]. The company produces approximately 36% of its steel in America, 53% in Europe and 11% in other countries[6]. In 2010, 65.6 million tons of steel were produced

through the (BOF) Basic Oxygen Furnace process and 21.8 million tons through (EAF) Electric Arc Furnace (furnace that heats recycled material by means of an electric arc)[6].

Arcelormittal Montréal produces semi-finished products, such as slabs and billets, and manufactures a wide range of high quality long steel products[7]. Production facilities in Contrecoeur, Quebec, have a direct reduction plant, two steel plants, a bar mill and a wire rod mill.

1.3 Process description at Arcelormittal

The Arcelormittal Contrecoeur West mini-mill site operates one steel plant with one electric arc furnace and a bar mill. This mill manufactures steel completely made out of recycled scrap steel.

Process flow at Arcelormittal Contrecoeur can be shortly described as (Figure 1):

1. Scrap charge
2. EAF- Electric Arc Furnace operation
3. Ladle refining
4. Continuous casting (strand casting).

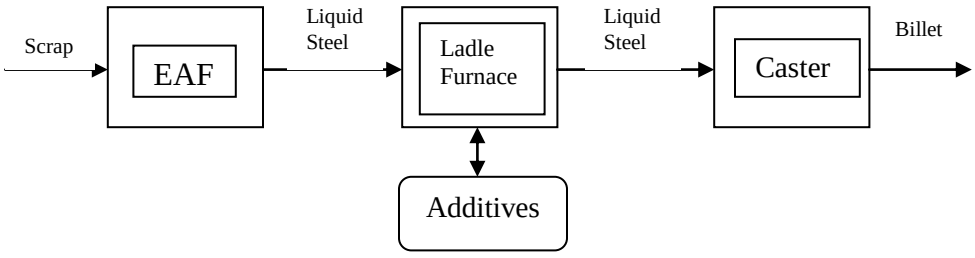

Figure 1: Steel production process

Although the process looks simple enough, each process step consists of many sub-processes and parameters which make the overall operation complex, time consuming and expensive. To briefly explain, Arcelormittal receives approximately 675,000 metric tons of scrap every year. Scrap metal is collected in a scrap bay, located next to the metal shop. Scrap is sorted into approximately 20 different grades including shredded, heavy

metal, stampings, steel clippings, DRI (direct-reduced iron: produced from direct reduction of iron ore) and tin. Depending on the type of grade, Arcelormittal designs a scrap recipe using specific types of scrap steel on a monthly basis.

Scrap is loaded into gondola cars using a crane of 20-ton capacity with a magnet capacity of 5 tons. A total of twelve loaded gondola cars are placed in front of the scrap bucket loading area. During every cycle cars are loaded, empty cars are removed, and replaced with filled cars. The sequences of cars in the scrap yard are scheduled according to the scrap recipe. Bucket loading refers to a process where each bucket is loaded with layers containing different types of scrap. Figure 2 illustrates the scrap loading bay at Arcelormittal Contrecoeur.

Figure 2: Scrap loading bay and scrap bucket at Arcelormittal Contrecoeur

Scrap recipes are designed based on desired grade and cost associated with the scrap. Arcelormittal uses a basic Excel model (Figure 3) developed by plant employees to design the recipe. Scrap grades and recipes are distinguished mainly on the content of Cu (Copper) in the steel.

					Recipes				Forecast		Corrected forecast		Utilization		
Type	Code	Cu (%)	Melt Yield (%)	Cost ($/T)	0.50-0.80%Cu max	0.35-0.40%Cu max	0.30%Cu max	0.25%Cu max	Quantity (T)	Quantity (%	Quantity (T)	Quantity (%	Quantity (T)	Quantity (%	%
DRI	408	0.00	0.880	403	0	0	0	0	0	0	0	#DIV/0!		#DIV/0!	0.00
Busheling	105, 126, 305	0.12	0.950	359	0	30000	60000	40000	9284	14.6	0	#DIV/0!		#DIV/0!	5.09
P&S	111	0.15	0.940	382	0	20000	30000	70000	5793	9.1	0	#DIV/0!		#DIV/0!	7.64
Frag	104, 204, 404, 504	0.35	0.925	401	60000	60000	70000	70000	17324	27.3	0	#DIV/0!		#DIV/0!	40.73
#1	101	0.37	0.900	336	70000	60000	30000	20000	12245	19.3	0	#DIV/0!		#DIV/0!	28.72
#2	112, 326	0.55	0.880	325	30000	20000	0	0	3284	5.2	0	#DIV/0!		#DIV/0!	
Tire wire	110	0.10	0.900	297	0	0	20000	20000	2872	4.5	0	#DIV/0!		#DIV/0!	
Turnings	123, 323	0.35	0.850	277	30000	20000	0	0	3284	5.2	0	#DIV/0!		#DIV/0!	
Tin cans	205	0.10	0.850	323	20000	0	0	0	1719	2.7	0	#DIV/0!		#DIV/0!	13.14
Fonte	509	0.04	0.740	336	0	0	0	0	0	0.0	0	#DIV/0!		#DIV/0!	
External skulls	109, 208, 209, 308, 508, 609,	0.06	0.850	196	30000	20000	0	20000	3674	5.8	0	#DIV/0!		#DIV/0!	
Internal skulls	108	0.30	0.850	14	0	0	10000	0	1241	2.0	0	#DIV/0!		#DIV/0!	
Billets	201	0.30	0.980	0	0	0	10000	0	1241	2.0	0	#DIV/0!		#DIV/0!	4.68
Rolled revert	202	0.30	0.980	336	0	10000	10000	0	1534	2.5	0	#DIV/0!		#DIV/0!	
				Charge (lbs)	240000	240000	240000	240000	63552	100.0	0	#DIV/0!	0	#DIV/0!	
				Cu (%)	0.32	0.30	0.24	0.21	0.27		#DIV/0!		#DIV/0!		
				Melt Yield(%)	88.71	90.92	92.94	92.31	91.25		#DIV/0!		#DIV/0!		
				Cost ($/T)	324.92	341.46	335.79	357.29	334.60		#DIV/0!		#DIV/0!		
									23,303,844				0		
				Forecast April 2011											
				Production (T)	18218	7480	26306	4134	56138						
				# Heats	172	71	248	39	530						
				Alloys (T)	1017										
				Yield (%)	86.94										
				Production April 2011											
				Production (T)					0						
				# Heats	0	0	0	0	0						
				Alloys (T)											

Figure 3: Screen shot of Excel model to calculate scrap recipe

Two or sometimes three buckets of scrap are used in sequence to load the EAF with 120 tons of steel (capacity). A crane loads the buckets located in two terminals of the scrap hall outside near the EAF. It takes 20 to 25 minutes to load one scrap bucket. Steel is loaded from the scrap bucket into the EAF. After the initial loading from the scrap bucket, the roof of the EAF is swung back and the 24" electrodes are placed into the scrap steel. During this initial process of scrap melting, a low voltage selection is beneficial to protect the crucible wall and roof refractory bricks. The voltage is increased as the process continues and the electrodes are raised[8]. Figure 4 shows the EAF furnace operation at Arcelormittal.

Figure 4: Melting process at Electric Arc Furnace

Oxygen is blown supersonically through one of the 3 Jet-boxes (PTI 1150SCFM) into the scrap, thereby combusting the steel. Wall-mounted oxygen fuel burners provide extra

heat, which accelerate the scrap meltdown. The process of oxygen charging and the conditions inside the furnace are controlled through a networked monitoring system at Arcelormittal that uses specific sensors and cameras. The process is fully controlled according to the conditions inside the EAF at any point of time[9]. Following this process, slag formation is the crucial part in steel making. Slags are materials floating on the surface of the liquid steel usually consisting of molten metal oxides and fluorides. The advantage of slag during steel making and the slag making process will be discussed in Section 2.

CaO (calcium oxide) and MgO (magnesium oxide) are used as basic additives and slag formers[10]. Injection of coke through a jet box into the slag layer reacts with iron oxide to form metallic iron and carbon monoxide gas. This is another crucial operation for making the slag to foam and shall be discussed in detail in Section 2.

Once the initial scrap has been completely melted, another scrap bucket is added to the EAF. After the second charge is completely melted, a refining operation is conducted to check and correct the steel chemistry. Slag formers are introduced and more oxygen is blown into the bath, burning out impurities such as silicon, sulfur, phosphorous aluminum, magnesium, and calcium. These formed oxides then become part of the slag[10, 11].

The secondary process usually known as ladle refining is the process after tapping the liquid steel from the EAF, where tapping is the removal of liquid steel into the ladle through a bottom tap hole of the electric arc furnace. Liquid steel in a ladle is then taken to a ladle metallurgy facility (LMF) with a capacity of 40 Megavolt Ampere (MVA). The goal of ladle refining is to deliver homogeneous liquid steel to the caster on time, at the right temperature and composition. Slag conditioning and the maintenance of slag quality in this process is an added advantage to produce better quality steel economically. Carryover slag from the furnace and flux addition during tapping promotes the development of slag in the ladle furnace[11, 12].

Ladle deoxidation occurs during the taping which helps alloys to combine with dissolved oxygen in the liquid metal to form SiO_2 and Al_2O_3[3, 13]. Injection of argon gas bubbled through bottom plugs are used to mix the liquid steel. Controlling the stirring rate is another parameter which should be controlled for better refining (explained in section 2.2.4.)

Alloy addition, desulfurization and maintaining the temperature of the ladle furnace are crucial parameters at the refining stage. Once the desired composition and temperature are achieved for casting, the ladle is transferred to the continuous casting facility. Arcelormittal has four continuous (strand) oil caster producing square billets ranging in cross section from 120-150 mm. Multiple tundishes with around 18 ton capacity are in rotation during the operation, where a tundish is a container with holes in the bottom to allow molten metal to enter into a mould. Tundish to mould steel flow is controlled using an orifice device, e.g., metering nozzles[14]. Different instruments and sensors are also used to have control over the level of liquid steel in the tundish.

Liquid steel is fed from the tundish to the mould at a regulated rate; the liquid steel slowly solidifies forming a solid outer shell and a liquid core. Mould oscillation is necessary during this process to avoid sticking and minimizes friction between the mould and the solidifying shell. This primary cooling area makes the metal cool sufficiently enough to form a shell of thickness around 0.4 to 0.8 inches[14]. The formed shell is withdrawn from the mould along with a dummy bar (curved metal beam used to track and lead the solidified strand) and the liquid steel continues to pour into the mould from the tundish. The withdrawal rate is currently controlled based on thickness, grade and level of the tundish, and is typically 80 to 130 inches per minute[14]. Casting time for one full tundish varies from 1 to 1.5 hours.

Upon exiting the mould the strands enter a secondary cooling zone where they are further cooled using water spray. Rollers and strengthener’s control the shape of the strands. All four strands at Arcelormittal are then cut with an oxygen cutter at a point where the steel billet is completely solid. The cut billets of required lengths are then stored and transported for further processing.

1.4 Project overview

The project was initiated by Arcelormittal Contrecoeur West with an optimistic vision to create an overall factory model that would optimize the whole steel making process. Processes like steel recipe selection, furnace loading, EAF, ladle furnace and casters needed improvements for efficient and economical operation. The factory model under development includes sub-models like:

- Cost Model: cost minimization in operations and material
- Production Model: optimization of steel production with regard to different modes of production defined by current steel market conditions
- Operational Model: optimization of steel making operations at each level of the process stream.
- Power Model - fine tuning and developing program with optimal slag.
- Chemical Energy Model – off gas measurement to optimize burners (oxygen fuel burners provide extra heat). EFSOP is an off-gas based process control technology for energy optimization by Tenova[15]. It is being used by Arcelormittal.
- Utilization model (maximizing raw material yield) incorporated with the scrap purchase model.

These sub-models connect together to make an overall EAF fusion model. These developments will benefit Arcelormittal to improve process time, production rate and product quality.

This thesis develops two different operational sub-models and is part of an overall EAF fusion model under development:
Part 1: Ladle furnace slag optimization model
Part 2: Caster productivity model
These two models are distinct.

1.5 Aim of the project

- **Part 1. Ladle furnace slag optimization for better refractory life**

The first objective is to develop a slag model to increase the efficiency of the steel refining process at the LMF (Ladle Metallurgy Facility). The model helps the process to reduce alloy consumption and maximize refractory life through MgO (Magnesium oxide) saturation.

Refractories are the primary materials used by the steel industry in the internal linings of the furnace to protect the furnace shell. Usually, basic refractories are used whose major content is magnesia (MgO), lime (CaO) or both. Studies have shown that refractories cover 20 % of the steel making production cost due to which there was a need to have control over the life of the refractory by saturating the slag with minimum magnesia or lime content to protect the refractories from chemical erosion.

The developed slag model will provide:

- the minimum weight percentage of MgO required in the slag for saturation based on the analyzed chemical composition of the slag
- the minimum amount of CaO required for desulfurization.

The model is based on reduced slag in the CaO-Al_2O_3-SiO_2-MgO system and uses empirical relations to calculate optical basicity and desulfurization. The MgO requirement to saturate the slag is based on calculated optical basicity (described in section 2.1.3). Slags at Arcelormittal are designed using CaF_2 as a fluidizer. CaF_2 in combination with lime and silica is effectively managed to deoxidize slag at the LMF. Solubility of CaO and MgO is strongly dependent on the type of fluidizer used. The addition of fluorspar to silicate slag results in an increased solubility of MgO in the slag. This effect is considered by maintaining CaO saturation[16, 17].

- **Part 2. Caster productivity improvement**

The second objective of the project is to develop an empirical model at the continuous casting zone to increase the casting throughput, while assuring that the core of the billet is solid when it is cut to avoid metal drain.

Presently, the casting speed at Arcelormittal is managed based on two parameters: liquid steel level in the tundish and predetermined billet length. This research task measured the cooling rate of the molten steel at the casting facility by systematic measurement of steel temperature at several points during the casting process for a sufficient number of distinct process instances. This data were then used to create a simulation model to predict the inner temperature profile of the steel based on the measured outer temperature.

A simulation model was developed using COMSOL Multiphysics 4.2, which is a finite element analysis and engineering simulation software developed by the COMSOL group. This software was used in the thesis to develop a 2D axisymmetric heat transfer analysis model. The model included the phase transition from liquid to solid in terms of latent heat. Simulation results provided data on temperature and phase distribution for the actual casting rate. Temperature measurements were compared to actual measured plant data to ultimately specify optimum casting rates for tested grades of steel.

Part – 1 Ladle Furnace Slag Optimization

Chapter 2 : Literature Review

2.1 Slag fundamentals

2.1.1 Definition of slag

"The scoria of a metal or fused material separated during the reduction of metal are called slag"[18]. Slags are material floating on the surface of the steel usually consisting of molten metal oxides and fluorides. The characteristics of the liquid fraction of the slag can be described as fluid, creamy, fluffy or solid[16].

The importance of slag has been very well understood by the steelmaking industry to cut the cost of producing quality steel. The slag phase is an essential part of the steelmaking process[16]. Tailoring the slag chemistry using concepts like "slag engineering or slag optimization" to improve the steel making process is a crucial part of making cost effective, quality steel. Enormous improvements in steel manufacturing techniques has been realized through thoughtful mechanism of metal, slag and gas reaction[19]. Because the primary purpose of slag is to absorb metallic impurities, the composition of slag is largely governed by the composition of the scrap steel and alloy recipe [19].

Techniques to remove impurities in the primary steel making process and modification through secondary refining techniques result in better yields, better quality steels and lower cost[19].

Remarkable benefits such as improved rate of melting, electrical efficiency, and reduction in arc radiation have led to the perception of "Make the slag and the steel will make itself."[20, 21]

2.1.2 Functions of slag

The basic properties of slag not only have an impact on the quality of steel and cost of manufacturing, but also on refractory wear[16].

Some important functions of slags are:

1. cover the arc produced by electrodes to protect the refractory from arc-flare,
2. protect the metal from oxidation,
3. control the steel oxygen levels and chemistry of the steel,
4. avoid oxygen and nitrogen pickup,
5. reduce temperature loss, and
6. help in dephosphorization and desulfurization [16, 20].

2.1.3 Slag formation

The melting process in the EAF furnace is followed by an oxidation stage, where formation of liquid slag is crucial. Liquid slag formation is facilitated either by the addition of wollastonite ($CaSiO_3$) or by the oxidation of silicon in the bath. FeO (Ferrous oxide) generated during the process is a powerful flux for rapid melting steel in the EAF[21].

The primary sources of slag formation are oxidation of metallic elements in the base metal such as manganese, silicon and aluminum, non-metallic elements such as sulfur and phosphorous, and minerals such as lime, spar and dolomite[20].

Oxygen blown into the melt promotes the oxidation stage. During this stage, excessive carbon, phosphorous, silicon and manganese oxidize to form magnesium oxide, carbon monoxide, silicon dioxide and diphosporus pentoxide[22].

$(FeO) = [Fe] + [O]$

$[C] + [O] = \{CO\}$

$[Si] + \{O_2\} = (SiO_2)$

$[Mn] + ½ \{O_2\} = (MnO)$

$2[P] + 5/2 \{O_2\} = (P_2O_5)$

Slag absorbs these oxides and carries them as waste. CO bubbles floating up in the melt help the process and refine the steel. Slag collected on the top surface of the molten steel in the furnace, enriched with oxides is removed, usually known as de-slagging[22].

After de-slagging at the EAF furnace, another slag making process is carried out at LMF, usually called the reducing stage or ladle refining. Slag here is mainly composed of CaO, CaF_2, and MgO. The function of slag here is to deoxidize and refine the steel from sulfur. Excessive oxygen is removed by metallic deoxidizers like manganese (Mn), silicon (Si), and aluminum (Al)[22].

$[Mn] + [O] = (MnO)$

$[Si] + 2[O] = (SiO_2)$

$2[Al] + 3[O] = (Al_2O_3)$

$[S] + (CaO) = (CaS) + [O]$

The purpose of secondary slag making is to protect the ladle furnace refractory and refine the steel to the required composition and temperature[16].

As there are many reactions during steelmaking that should be considered, balancing the reaction in order to control the oxygen level in the furnace or the ladle is hence very important. Therefore, controlling the oxygen activity through balanced formation of FeO is crucial for better slag design and steel composition[20].

Other ideologies to form a good slag and to avoid refractory erosion are: minimum slag formation at EAF, MgO saturated slag with B4 basicity of 1.8 to 2.3 and foam at the right time (i.e., fluffy to creamy slag)[16, 20].

Thus, it is very important for engineers and scientists to find a general composition factor that can be applied to slag. The most common method is to use basicity index.

2.1.4 Slag basicity and optical basicity

"Basicity is defined as the ratio of basic and acidic oxides in iron ore material."[23]

"Slag basicity is a means by which steelmakers refer to how acid or how basic slag is in relationship to the basic refractory utilized in the furnace or ladle vessels."[20]

Most of the slag line refractories are basic so MgO and/or CaO saturation is required to avoid refractory damage. Saturating slags with these oxides is also vital for good foaming; hence, based on the required foaming level and to protect the refractories, the slag must be dual saturated or must be at least MgO saturated[11].

Typical slag components with melting points are as listed in Table 1. In the list, oxides can be split into two types, refractory oxides such as CaO and MgO and fluxing oxides consisting of SiO_2, $Al2O_3$, FeO, MnO and CaF_2[11]. The effective viscosity of the slag increases by addition of refractory oxides beyond the liquidus composition, whereas addition of fluxing oxides increases the fluidity of the slag[11].

Table 1: Slag components

Oxide	**Melting Point (C)**
SiO_2	1720
CaO	2600
MgO	2800
Al_2O_3	2030
FeO	1370
MnO	1850
Cr_2O_3	2260
CaF_2	1420

The balance between refractory oxides and fluxing oxides effects slags that are compatible with basic refractories and also able to attain the desired foaming requirements[11]. Due to the lower strength of fluxing oxides and different effects on the solubility of CaO and MgO in the slag, the process of balancing the two oxides is very complex[11].

Slag basicity defines the balance between the refractory oxides and the fluxing oxides. A basicity ratio, called 'V' ratio (%CaO / %SiO2), is the first estimate and commonly used. Slags containing other oxides like MgO, Al_2O_3, TiO_2 and CaF_2 are defined using other formulations[16].

B_3= %CaO / (%SiO_2+% Al_2O_3+%TiO_2)[20]
B_4= (%CaO+%MgO) / (%SiO_2+% Al_2O_3+% TiO_2)[20]
B_5= (%CaO+%MgO) / (%SiO_2+% Al_2O_3+%CaF_2)[20]

The B_5 ratio can also have acidic components FeO and MnO, where it is important to keep their sum less than 5%[16].

B3 and B5 ratios are still being used in steelmaking, but the problem with basic basicity types is that it gives an arbitrary decision whether the slag is basic or acidic and does not include differences in the relative basicities/acidities of the different oxides [16].

Optical basicity:

"Optical basicity" was first introduced by Duffy and Ingram[24]. Optical basicity (Λ) was based on Lewis acidity/basicity assigned to a variety of oxide media making it possible to compare the basicity of oxide media[24]. Duffy and Ingram [25] noticed "*frequency shifts in the ultraviolet (s-p) spectra of probe ions such as* Pb^{2+} *can be expressed on the numerical scale of optical basicity*". It was also noted that these spectra can be related to the chemical behavior of slags[26].

Duffy and Ingram in their later work [27] stated that in the slag system, basicity can be expressed in terms of electron donor power as an optical basicity. The optical basicity

was defined using equation $\Lambda = \Sigma X_i \Lambda_i$, where X_i and Λ_i are equivalent basicity values for slag components.

Optical basicities of various slag systems are determined from their Pauling electro-negativities[27]. The average optical basicity for a slag of any composition can be calculated by means of Equation (1) [16]

$$\Lambda = X_a.\Lambda_{th\,(a)} + X_b.\Lambda_{th\,(b)} \qquad (1)$$

where Λ is the optical basicity of the slag and Λ_{th} is the optical basicity of individual oxides defined in Table 2[16],

and $$X = \frac{mole\ fraction\ of\ component * number\ of\ oxygen\ atoms\ in\ oxide\ molecule}{\Sigma\ mole\ fraction\ of\ component * number\ of\ oxygens\ in\ oxide\ molecules\ of\ all\ components}$$

Thus, in CaO-Al_2O_3-SiO_2 slag,

$$X_{CaO} = \frac{NCaO}{NCaO + 3NAl2O3 + 2NSiO2}$$

$$X_{Al2O3} = \frac{3NAl2O3}{NCao + 3NAl2O3 + 2NSio2}$$

$$X_{SiO2} = \frac{2NSio2}{NCaO + 3NAl2O3 + 2NsiO2}$$

Table 2: Optical values of slag components

Oxide	Optical Basicity
Na_2o	1.15
CaO	1.0
MgO	0.78
CaF_2	0.67
TiO_2	0.61
Al_2O_3	0.61
MnO	0.59
$Cr2O_3$	0.55
FeO	0.51
$Fe2O_3$	0.48
SiO_2	0.48

Although optical basicity is not useful in predicting the physical properties of the slag, it is the best compositional parameter available to describe the composition of a slag. The only exception being that the optical basicity concept is only useful, if the slag is completely fluid[16].

2.1.5 Slag viscosity

In addition to the importance of slag in steelmaking, slag foaming is another important parameter to be considered for lowering refractory wear and electrode consumption. Eugene Pretorius has defined possible ways of having control over the foaminess and obtaining optimum foamy slags [11].

Eugene Pretorius explained that the presence of second phase particles in the slag has greater impact on foaming than slag tension and slag viscosity, i.e., to have balance between refractory and fluxing oxides. He also mentioned that second phase particles serve as gas nucleation sites leading to formation of small gas bubbles[11].

Effective viscosity in relation to the amount of second phase particles in the slag and viscosity is defined as in Equation (2)[11, 28]:

$$\eta_e = \eta\,(1 - 1.35\,\Theta)^{-5/2} \quad (2)$$

where:

η_e- effective viscosity of the slag

η - viscosity of the molten slag

Θ - fraction of precipitated solid phases.

As we know, the main four variables affecting slag are: basicity, FeO content, MgO content and temperature, it is quite obvious that these variables also have their influence on the foaminess of the slag. The relation between optical basicity and viscosity can be shown based on the experimental work of D. Ghosh on the CaO-SiO_2-Al_2O_3 system [26]. As shown in Figure 5 below, it can be stated that viscosity decreases when optical basicity increases, which guides us to keep low silica and alumina content in the slag by using excess lime[26].

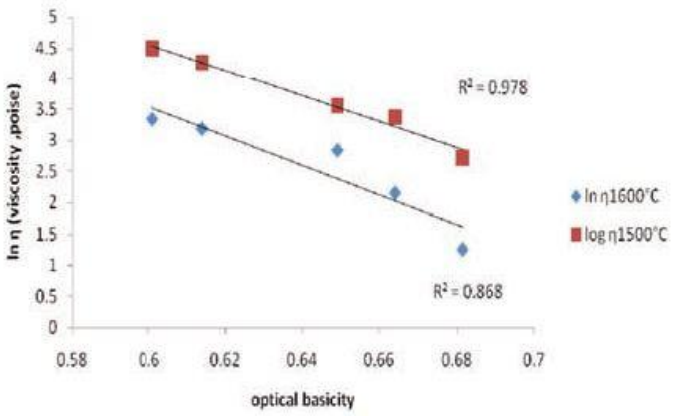

Figure 5: Optical basicity versus slag viscosity [26]

Similarly, the relation between the liquidus temperature of slag and optical basicity was also observed (Figure 6). It was noticed that the liquidus temperature of the slag increases as optical basicity increases. This also leads to logic that increasing lime addition may increase the liquidus temperature of the slag[26].

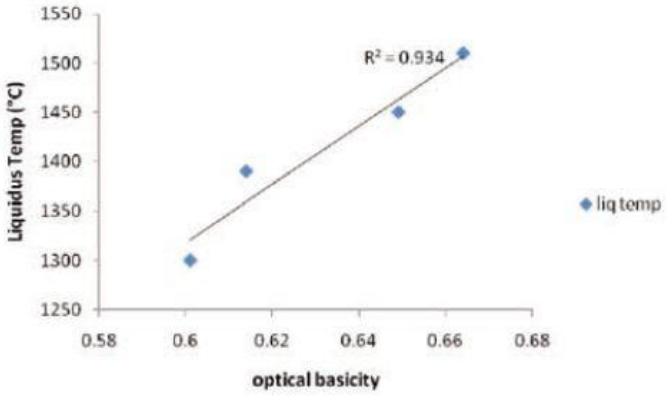

Figure 6: Optical basicity versus liquidus temperature of the slag[26]

2.1.6 Slag requirements for refractories

The most important and primary objective of making a slag to produce better steel is to balance the slag. Balance between refractory oxides CaO, MgO and fluxing oxides like SiO_2, Al_2O_3, and CaF2, is crucial. With CaO (2600°C) and MgO (2800°C), the addition of other flux additives is required to form a liquid slag at steel making temperatures[16].

Slag engineering keeps the slag balanced between refractory oxides and fluxing oxides, making it creamy for refractory protection and metallurgical requirements. Eugene Pretorius mentioned that a minimum B5 basicity ratio of 1.5 is required (60% refractory oxides and 40 % fluxing oxides) to obtain a reasonable ladle slag[16].

Depending on the content of refractory oxides, slag can be classified as crusty, having too much of CaO/MgO. A fluffy slag with saturated CaO/MgO is good for refractories, but not optimum for desulfurization. Watery slags which contain too little CaO/MgO make the slags very aggressive and they harm the refractory by depleting manganese. Creamy slag just saturated with CaO/MgO is known to be the ideal slag for a better steelmaking process[16]. CaO-Al_2O_3 phase diagram (Figure 7) can be referred to classify the consistency of slags.

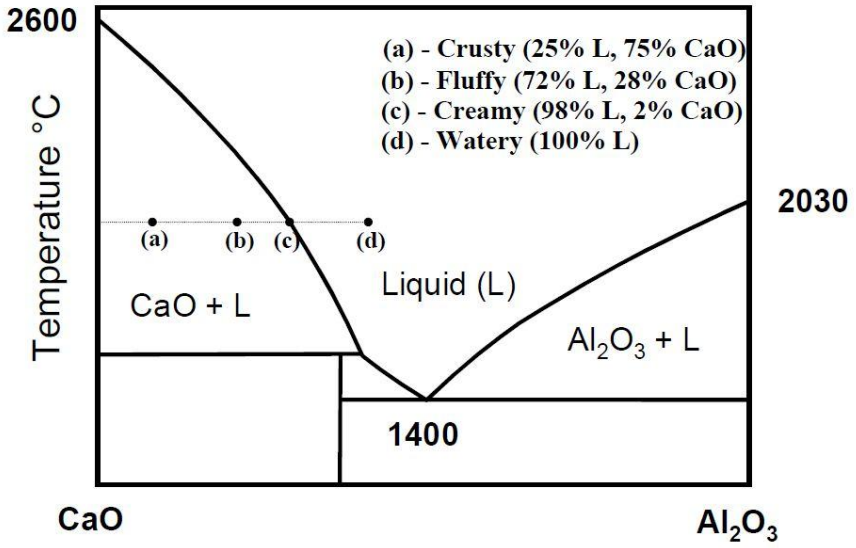

Figure 7: Phase diagram for the system CaO-Al_2O_3[16]

The main wear mechanism of the ladle refractory slag line is chemical corrosion and mechanical erosion due to stirring of the liquid steel. Chemical wear is mainly due to the difference of chemical potential between the refractory and the slag under high temperature conditions. Hence, the process of slag making is supported by many variables like temperature, slag thickness, refractory composition, slag composition and stirring rate making the process very complex[29].

2.2 Secondary steel making

As stated earlier, the goal of ladle refining is to provide liquid steel on time at the right temperature and chemical composition to the caster. We explore more about secondary steelmaking (ladle refining) in this section as it is of much importance towards the objectives of this project.

There has been significant development in secondary steelmaking in recent years; a high level of investment to develop new secondary steelmaking facilities has been made by many steel manufacturers. The reason is the possibility of handling complex tasks like the fine adjustment of composition, temperature and steel cleanness at secondary steelmaking processes[30]. Better control over process metallurgy due to secondary steelmaking

operations has led to the development of new products and improvement in the quality of steel.

As in the case of EAF, it is also very important to obtain conditioned slag during the secondary steelmaking process. Many benefits are realized due to the sequence of events at the ladle furnace such as, the addition of suitable fluxes for good fluidity and slag volume during the tap, the addition of deoxidizers for better alloy recoveries, creamy slag with improved desulfurization ability, and thermal efficiency. The sequence of ladle refining also benefits the slag to be able to absorb inclusions making the steel cleaner[16]. Further, the addition of lime to maintain the creamy slag consistency provides better refractory life.

Some of the important secondary steelmaking processes like deoxidation, ladle injection, vacuum degassing, stirring, desulfurization and ladle reheating assist the sequence of ladle refining and the slag making process[30]. Knowledge of these processes helps to understand and implement techniques towards the objective of developing an optimized slag model.

Generally, ladle slags are generated by carryover slag from the furnace, additions from fluxes such as lime, dolomitic lime (calcium magnesium carbonate) and CaF_2/sand.

2.2.1 Carry over Slag

Slag containing impurities during the primary steel refining at EAF is carried over to the ladle when the steel is tapped. This carryover slag was considered undesirable, as the impurities can revert to the steel in the ladle. It has always been an important issue to control the consistency and level of slag carryover.

Eugene Pretorius in his study[16] clarified that carryover slag can be tolerated in the ladle furnace depending on the quality and the grade of the produced steel. In steels like reinforcing bar, slag plays a very limited role due to the high phosphorous and sulfur content in the steel. In this case carryover slag has an advantage. The main benefit of promoting carryover slag is that the carryover slag is already hot and mostly liquid where

it can act as a fluxing precursor. Lime addition to this slag can neutralize the slag to improve refractory compatibility[16]. Depending on the requirement many steel manufacturers use different methods to eliminate or minimize the carryover slag in the ladle. In some cases well conditioned slag carryover can be tolerated and can even be beneficial.

2.2.2 Deoxidation

Oxygen injected at the EAF for refining and slag foaming often increases the oxygen content in the steel. Tapped steel in the ladle with high oxygen content has to be deoxidized so as to achieve better steel composition and to have better alloying.

Deoxidation can be achieved by initial addition of alloys during the taping of steel from the furnace called precipitation deoxidation which helps mixing of the steel and alloys to achieve deoxidation[20]. Precipitation of Al_2O_3 and SiO_2 is due to ferrosilicon and aluminum combination with dissolved oxygen[20]. If the dissolved oxygen content in the form of FeO and MnO still exists in the deoxidized steel, this has to be treated with deoxidizers to reduce the oxygen activity of the slag. This reduction process is called diffusion deoxidation[20]. Low oxygen activity in steel is very important as it benefits ladle refining, alloying and desulfurization process.

2.2.3 Ladle injections

Injection of chemical powders into the steel to produce low sulfur steels was an important development in the 1960's[30]. Sulfide inclusions bring many operation problems and quality issues for which treatment with calcium silicide has become an essential part of the refining process. Lime injection is also used as a means to reduce sulfur levels[30].

2.2.4 Stirring

The ladle furnace is usually equipped with a stirring facility, either electromagnetic or gas stirring. Stirring is important for good metal/slag interaction to achieve an effective ladle refining. It also helps inclusion removal and enhances the temperature and composition of the steel[30].

The gas stirring rate should be controlled very precisely to accomplish better operation. Very low stirring rate leads to superheating of the slag which erodes the refractory. On the other hand excessive stirring can cause carbon pickup and short circuiting, where short circuiting is caused by the presence of a foreign object or conductive dust[31]. Better thermal efficiency can be achieved at lower stir rates, whereas for alloy addition and desulfurization higher stir rates are beneficial[16].

2.2.5 Slag for secondary steel making

In a nutshell, the basic rule to optimize the slag for the ladle metallurgy facility is:

- limit slag carryover to the ladle,
- reduce FeO and MnO content to less than 1%, which is corrosive to ladle brick and carries oxygen to the steel,
- maintain basic slag of 2.5(B5 basicity ratio) or higher by having creamy consistency of slag,
- and to have slag with the correct amount of lime and MgO to enhance desulfurization and to protect refractories[20].

In practice, the appearance of a slag provides useful information on the amount of reducible oxide it carries. It is always appreciated to avoid dark oxides like FeO, MnO and Cr_2O_3 for cleaner low oxygen content steel[20].

2.3 Desulfurization

Sulfur content in steel is reduced to its minimum because of the negative effects on physical and mechanical properties. Sulfide formation in steel generates cracks in the steel during solidification[20]**.** Sulfur possesses a considerable likeness for manganese; it forms MnS, which results in inclusions in the steel, thereby degrading the steel.

Desulfurization can be done at several points in the steelmaking process using different reagents, but usually desulfurization is carried during the reducing stage when the oxygen activity of the steel is low[32].

Desulfurization is always preferred at higher temperatures and good stirring conditions to have better slag and metal interaction. Reaction of the desulfurization process can be as shown in Equation (3)[20],

$$2CaO_{(Slag)} + 3\,FeS_{[Steel]} + CaC2 \longrightarrow 3CaS_{(Slag)} + 3Fe_{[steel]} + 2CO \qquad (3)$$

It is very important to note that sulfur in steel is only removed by lime that is dissolved in the liquid portion of the slag[16, 33].

2.3.1 Thermodynamic principal

Sulfur transfer from metal to the slag is governed by the reaction shown below[32],

$$[S] + (O^{-2}) < - > (S^{-2}) + [O]$$

where notations in the [] brackets denote content in the metal and notations in the () brackets denote content dissolved in slag.

Gas slag equilibrium techniques based on the following reaction are used to experimentally determine the equilibrium constants (K)[33, 34].

$$½\ S^{2} + O^{-2} + S^{-2} + ½\ O^{2}$$

$$K = \frac{a_{S^{-2}}}{a_{O^{-2}}} \cdot \sqrt{\frac{P_{O_2}}{P_{S_2}}}$$

$$K = \frac{f_{S^{-2}} \cdot (\%S)}{a_{O^{-2}}} \cdot \sqrt{\frac{P_{O_2}}{P_{S_2}}}$$

where $a_{S^{-2}}$ and $a_{O^{-2}}$ are the activities of sulfide and oxide in the slag. The sulfide capacity (Cs) can be calculated using Equation (4), which is based on the equilibrium constant[33, 34].

$$Cs = \frac{K_6 . a_{O^{-2}}}{f_{S^{-2}}}$$

$$Cs = (\%S) \cdot \sqrt{\frac{P_{O_2}}{P_{S_2}}} \quad (4)$$

2.3.2 Sulfide capacity

Sulfide capacity (C_s) describes the slag's potential ability to remove sulfur from steel[33]. This important property of slag is very useful in prediction and control of the desulfurization process[32]. Sulfide capacities are expressed in log units. The less negative the logarithmic unit, the better the sulfur removing capacity of the slag. Sulfide capacities for $CaO\text{-}Al_2O_3\text{-}MgO$ and $CaO\text{-}Al_2O_3\text{-}SiO_2$ systems, determined experimentally, are as shown in Figure 8 and Figure 9[33].

These experimentally determined sulfide capacities are not useful for complex industrial slags, where a general expression of 'C_s' as a function of slag composition and temperature would be useful. Correlation of optical basicity with sulfide capacity has shown very good correspondence over a wide range of slag composition[32, 33].

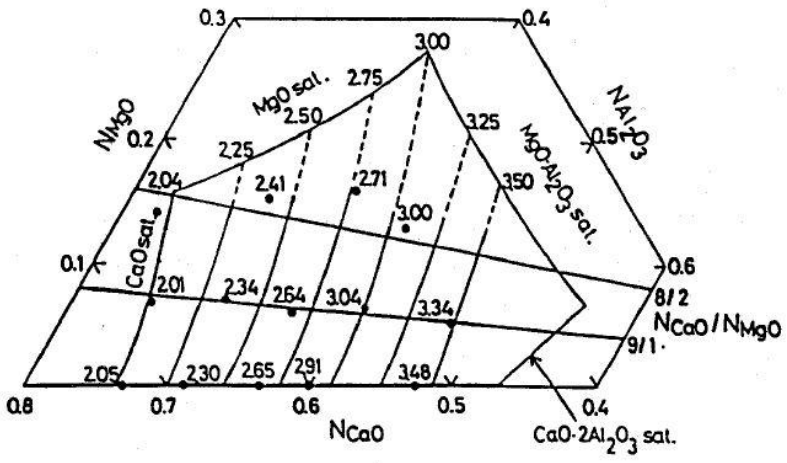

Figure 8: Iso-Sulfide capacity curves for $CaO\text{-}Al_2O_3\text{-}MgO$ slags at 1600°C[33]

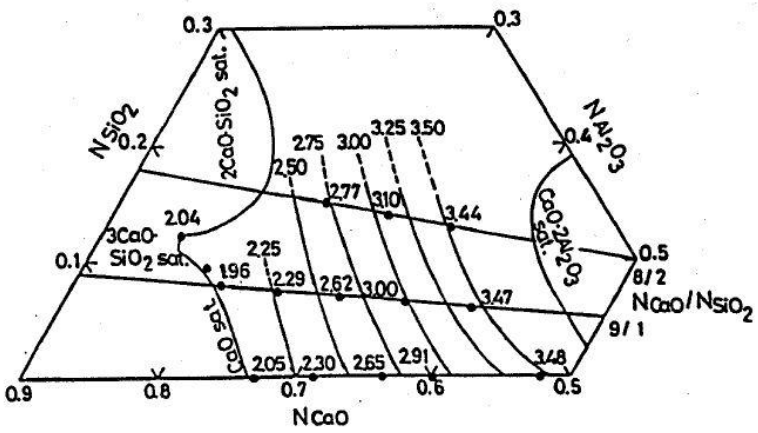

Figure 9: Iso-Sulfide capacity curves for $CaO-Al_2O_3-SiO_2$ slags at 1600°C

2.3.3 Correlation of sulfide capacity with optical basicity

Sosinky and Sommerville had proposed a sulfide capacity prediction model using the optical basicity concept defined by Duffy and Ingram[24, 34].

The relation between sulfide capacity and optical basicity is given by Equation (5):

$$\log C_s = \frac{[22690-(54640*\Lambda)]}{T} + [(43.6 * \Lambda) - 25.2] \quad (5)$$

where optical basicity is calculated using Equation (1).

Various adjustments have been proposed in an effort to improve accuracy of the correlation with optical basicity. Alternate correlations that are not based on optical basicity are also available, but are less useful. The optical basicity correlation is easy to use and shows good approximation for different ranges of slag composition.

2.3.4 Sulfur distribution ratio

The ratio of sulfur content in the slag and the metal phase usually describes an estimation of the sulfur reduction in a desulfurization process. The relationship between Cs and Ls (sulfur distribution ratio) can be as shown:

$$L_s = (C_s)\frac{K}{[\%O]}$$

where [%O] is the oxygen content in steel and K is the equilibrium constant.

This relation can be used to derive the equation in the logarithmic form as shown in Equation (6). Thus, Ls (sulfur distribution ratio) is a function of temperature, sulfide capacity, oxygen activity and sulfur content of the molten steel[32, 33].

$$\log L_s = \log \frac{(\%S)}{[\%S]} = \frac{-935}{T} + 1.375 + \log C_s + \log f_s - \log a_o \quad (6)$$

where f_s and a_o are the activity coefficient of sulfur and oxygen activity in the metal and the value of equilibrium constant was considered as logK= -935/T+1.375.

If the sulfur and oxygen content in steel are known, L_s (sulfur distribution ratio) can be calculated using values of C_s (sulfide capacity) for a particular slag.

It is always assumed that L_s values should be large for better sulfur removal. This can be achieved by having high temperature, large C_s value and low oxygen activity[33]. Since the sulfide capacity and sulfur distribution ratio are functions of temperature, it is very important to maintain high temperatures for a better desulfurization process[32].

2.3.5 Equilibrium Sulfur and Sulfur removal degree

According to Equation (7):

$$[\%Seq] = \frac{[\%S]*W_m}{W_m + L_s * W_{slag}} \quad (7)$$

slag and metal weight (W_m and W_{slag}) and initial sulfur content in the metal (%S) affect the final sulfur content[33]. Also, to have lower final sulfur content in the metal, the value of L_s should be high or slag volume should be high, or alternatively the initial sulfur content should be low. Also, the degree of sulfur removal η_S during desulphurization treatment is a very capable tool to characterize the efficiency of the treatment with slag. It is given by Equation (8),

$$\eta_s = \frac{[\%S]i - [\%S]f}{[\%S]i} . 100\% \quad (8)$$

2.4 Designing the slag recipes

The ternary systems can be used to evaluate the fluxing effect of oxides on CaO and MgO. For example, the CaO-SiO_2-MgO phase diagram can be used to evaluate the effect of SiO_2 on CaO and MgO. The phase relation as a function of temperature and composition for any mixture can be utilized. Figure 10 shows a simple isothermal section of a CaO-SiO_2-MgO system at 1600°C[16].

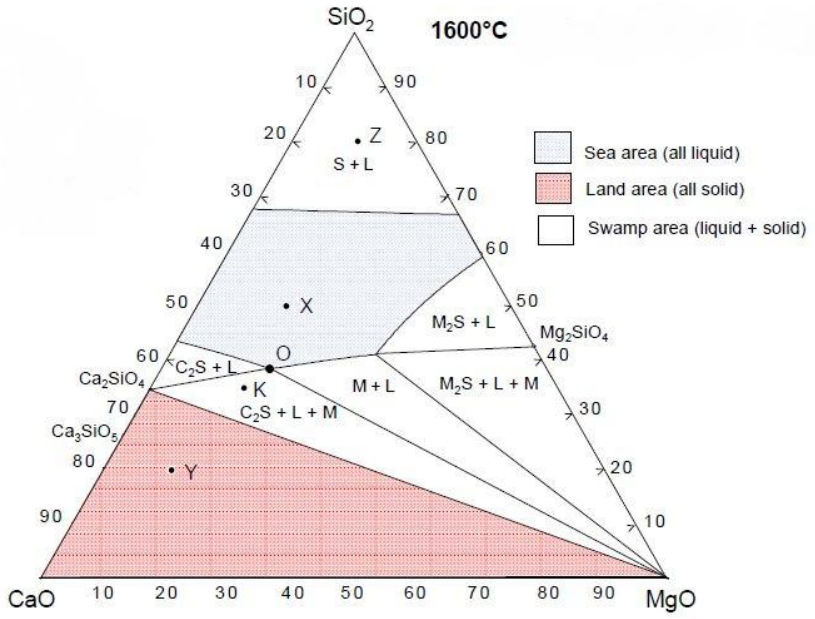

Figure 10: Isothermal section of CaO-SiO_2-MgO system[16]

2.4.1 Slag requirement for Magnesia-Carbon slag line

Consider Figure 11 where the solid line through points O to P to Q indicates that slags are MgO saturated[11, 16]. For any slag to be compatible with the magnesia-carbon slag line it has to be on the saturation line as shown. It can be easily inferred from the graph that solubility of MgO is a function of slag composition. Also it is noted that the MgO

saturation value is at its minimum when the slag is also CaO saturated (Point O)[16]. This means that the MgO dissolution in the brick is lowest when the slag is also CaO saturated.

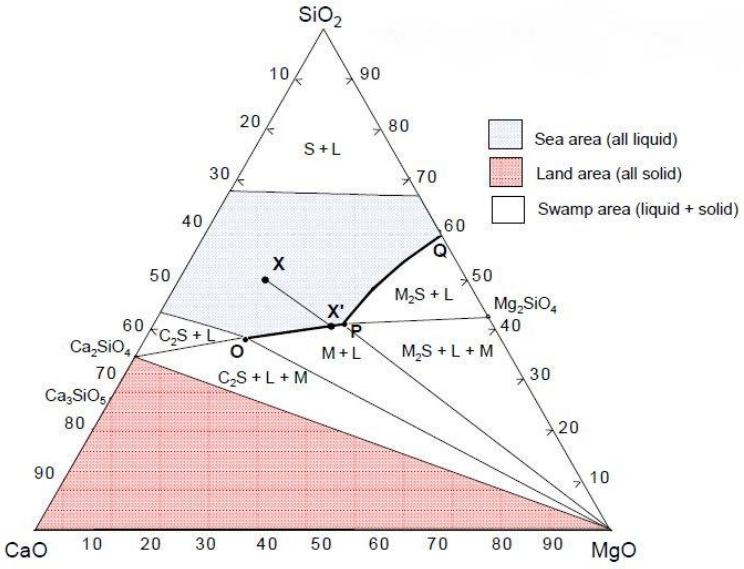

Figure 11: MgO saturation O-P-Q at 1600°C[16]

Figure 12 shows a plot of the solubility of MgO as a function of slag basicity. There is a very large increase in the MgO solubility as the basicity of the slag decreases.

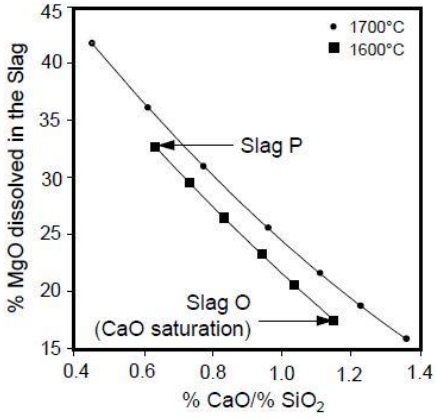

Figure 12: MgO solubility versus basicity at 1600°C and 1700°C[16]

Similar saturation relations can be demonstrated for dolomite refractories showing the CaO saturation zones. For the interest of this project we only consider the effect of slag composition on MgO solubility, as the refractories at Arcelormittal are magnesia based.

This also supports the fact that we need to also consider the minimum CaO saturation required if different fluidizers are used.

Studies on the effect of Al_2O_3 over CaO and MgO solubility considering the CaO-Al_2O_3-MgO system at 1600°C showed some interesting specifics. It was noticed that CaO solubility was higher in the CaO-Al_2O_3-MgO system than the CaO-SiO_2-MgO system indicating that Al_2O_3 was a better flux for CaO than SiO_2[16]. On the contrary, solubility of MgO is much lower in the CaO-MgO-Al_2O_3 system. Eugene Pretorius showed the relationship of MgO solubility with silicate slag and aluminate slag (Figure 13)[16]. It can be noticed that MgO solubility is much higher for silicate slags for different basicity ratios.

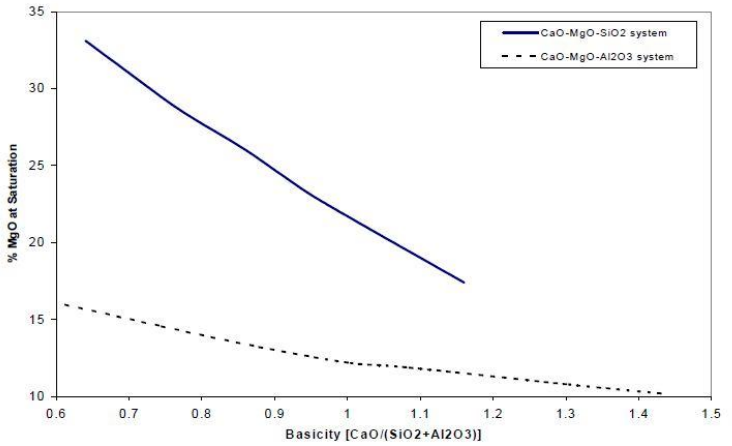

Figure 13: Solubility of MgO in CaO-SiO_2-MgO and CaO-Al_2O_3-MgO system at 1600°C[16]

2.4.2 CaO-MgO-Al_2O_3-SiO_2 system

The slags containing both SiO_2 and Al_2O_3 as fluxes use the quaternary system CaO-Al_2O_3-SiO_2-MgO, as ternary phase diagrams are of limited use to demonstrate slag fundamentals and their direct application to steelmaking slags[16]. A quaternary system is more complex, but can be simplified for the applicability of slags that are of interest.

Slags with high CaO solubility for better desulfurization and compatibility to both magnesia and dolomite refractories are considered optimum for steelmaking. Dual saturated slags showing the variation of CaO and MgO solubility as a function of Al_2O_3 content can be graphically shown as in Figure 14 [16]. Alumina acts as a flux to bring the added lime into solution, i.e., Al (Aluminum) killed steels have high fluidity and better sulfur removal properties[16, 33].

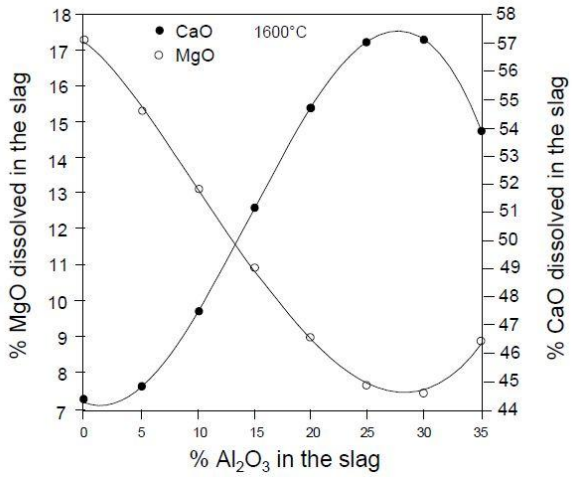

Figure 14: CaO and MgO solubility as a function of Al_2O_3 content in quaternary system at 1600° C[16]

Phase diagrams and different slag models can be used to design slags based on required metallurgical goals. The solubility of CaO and MgO strongly depends on the type of fluidizing agent used (SiO_2, Al_2O_3, CaF_2)[33]. Slag fluidity and compatibility with ladle refractories are guiding tools to design slag recipes to meet metallurgical requirements with varying sulfide capacity.

2.5 Research and slag models

Historical development of slag models showing techniques that were developed to control slag were achieved by establishing empirical correlation between the chemical components and metallurgical chemistries. Use of basicity ratios was the outcome of the development[35]. “Baker refractories introduced its first PC-based phase calculation program based on Rait’s work in 1986.”[35] It was then that computer applications to

evaluate parameters of the steelmaking process were first realized. Since then computer programs have become an essential tool in controlling the process and making the adjustments to achieve steelmaking goals[35].

Some models developed for EAF furnace slag optimization showed the route towards development of obtaining better slag for a ladle furnace. Phase relations and thermodynamic approach was used for the study.

James et al. [36] in his study on obtaining optimum slag chemistry and viscosity mentioned that foamy slag practices could save energy by 3-10% and refractory consumption by 25-63%. His work was based on the quaternary oxide system of MgO-CaO-FeO-SiO_2 and the thermodynamic program, FactSage, (FactSage is one of the largest database systems in chemical thermodynamics that permits the calculation, plotting, and editing of multi-component phase diagrams.)[37]. Factstage was used to predict the dual saturation level of CaO and MgO and the saturation level of MgO with variation of oxygen partial pressure, operational temperature, and slag basicity. Results indicated a linear relationship among oxide components, basicity, and acidity which made predicting optimum slag chemistry possible.

Eugene Pretorius [16] proposed an isothermal stability diagram (ISD) for simple systems such as MgO-CaO-SiO_2-FeO with basicity representation. Slag compositions were calculated through the ISD representation.

The Albany Research Center (ARC) [38] has developed a model which predicts foaming slag chemistry. Use of this model extends refractory life, saves energy and gives better control of foamy slag chemistry. The ARC model can predict saturated EAF slag chemistry based on the linear relationship between atomic percentages of oxides and slag basicity ratios. MgO saturated EAF slag chemistry can be derived from the dual saturated EAF slag chemistry and the known FeO content in the slag.

Another research on degradation of MgO showed few important considerations. Nightingale et al., 2005, [39] in his experiments on exposure of MgO to slags under forced convection flow condition showed different degradation mechanisms. The role of

Al_2O_3 in the degradation process was assessed. It was seen that loss of MgO was reduced at 1500°C due to the formation of a spinel layer. It was concluded that strength of the bond between spinel and underlying MgO played an important role in degradation of MgO refractories.

Many slag models were developed to be used on personal computers like the one based on solidus phase relation and Rait's mineralogical work[35, 40]. The models were not useful as they did not show the effect of temperature variation on the solubility of CaO and MgO[35].

A slag model based on multi-dimensional phase equilibria utilizing a statistical and mathematical approach to demonstrate the liquidus and solidus phase relations as a function of temperature and composition are of much interest these days[35]. Optical basicity correlations are used to estimate desulfurization and to calculate CaO/MgO saturation levels. Eugene developed [35] two models, the first was applicable to EAF slag modeling for better foaming and compatibility with magnesia-slag line refractories. The second model was for reduced slag applicable to ladle slags. Slags compatible with magnesia and dolomite refractories just saturated with MgO or both CaO and MgO with various combinations of fluidizers can be designed using this model[11, 16, 35].

Our objective of this thesis is to design a model for the ladle furnace slags for better refractory life. The model considers the quaternary CaO-SiO_2-AL_2O_3-MgO system with intake of knowledge from latest developments and Eugene's reduced slag model.

Chapter 3 : Methodology

The literature review gave a detailed discussion on different concepts and recent research that were made on ladle furnace slag optimization. This thesis brings together a few techniques and concepts to build a slag model that calculates MgO required for saturation. This section describes the methodology that was followed to build the slag model for ladle furnace.

The slag model was initially built to calculate the MgO saturation level for the analyzed slag based on the optical basicity. The model was then extended to calculate the MgO required for saturation considering the desulfurization process. The following demonstrates the working of the model and the considerations that were made.

3.1 The basic structure of the model

The steel plant at Arcelormittal Contrecoeur is characterized by high productivity, an average of 20 heats per day. It is very important for the company to extend the refractory life due to its high replacement cost and the operation downtime incurred. Studies have shown that cost of the refractories are around 20% of the steelmaking production cost[41].

The initial aim of the model was to increase the operating life of magnesia based refractories by keeping the slag saturated with MgO.

In this prospect, the model considers:

- optical basicity calculation based on analyzed slag data
- MgO saturation level determined through the calculated optical basicity.

The extended slag model included the desulfurization process and considered the fact that the addition of additives to control the desulfurization process changed the optical basicity concentration. This caused variation in the MgO requirement, which forced recalculation of the minimum amount of MgO for a new value of optical basicity.

Desulfurization is driven by low oxygen [O] in the steel and high CaO activity in the slag, that is, a high CaO/SiO_2 ratio and a low SiO_2 activity in the slag[16]. Also, it is very important to consider the fact that it is only the liquid portion of the slag carrying CaO that participates in the desulfurization process[33]. This indicates that for deep desulfurization the liquid portion of the slag must contain as much CaO as possible at the expense of MgO, but not to the extent that the refractory compatibility with the slag is compromised.

Hence, the model iteratively changes the CaO by adding lime until the desired level of sulfur [S] in the steel is reached. As described, this goes well with liquid and fluid slag with high sulfide capacity (C_s), high temperature and decent slag volume. This slag model only calculates the MgO required based on changing optical basicity and does not improve the efficiency of the desulfurization process. Slag consistency and slags for efficient desulfurization can be achieved by using desulfurization models already available at Arcelormittal and other work methods. Thus, a model that optimizes the concentration of MgO and the efficiency of the desulfurization process is proposed as defined in Figure 15.

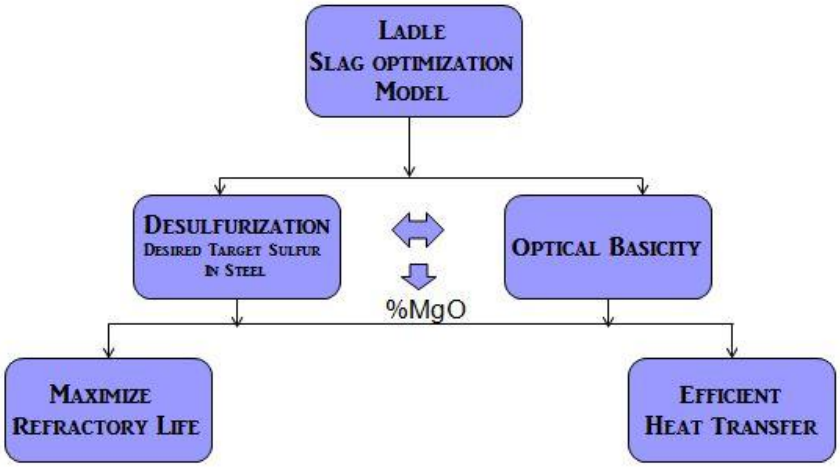

Figure 15: Structure of the slag model

3.2 Description of the slag model

As described earlier the main objective of the slag model is to determine the MgO saturation level for the magnesia slag line. The following parameters are required as the model data for calculation:

- steel weight and the slag volume contained in the vessel after the slag analysis,
- slag analysis result showing the chemical composition of the slag,
- temperature of the liquid steel,
- oxygen content (ppm-parts per million),

- initial sulfur content in the steel,
- target sulfur required.

The required input data as listed above are given in Table 3 with associated constraints.

Table 3: List of model inputs

Slag composition and other data	**Constraints**
Analyzed Slag Composition	All components add up to a value between 95 to 100 wt%, where wt% is the percentage by weight.
Temperature	Model works well at 1600 C, but can be extended to 1700 C
Metal Weight	-
Slag weight	-
Oxygen (ppm)	-
Oxygen activity	Calculated based on oxygen ppm provided as ^{a}O = [%O] = ppm [O]/10000.[33]

3.2.1 Determination of optical basicity

Using the data of the slag analysis, optical basicity can be calculated based on Equation (1), as explained in section 2.1.3.

$$\Lambda = X_a.\Lambda_{th\ (a)} + X_b.\Lambda_{th\ (b)}$$

3.2.2 Determination of MgO saturation level

Further to the discussion in section 2.4 on $CaO\text{-}Al_2O_3\text{-}MgO\text{-}SiO_2$ slags, MgO solubility can be determined. From Figure 16 it is noticed that MgO solubility decreases as optical basicity value increases. This is due to the fact that MgO solubility is low when the slag is CaO saturated[11, 16].

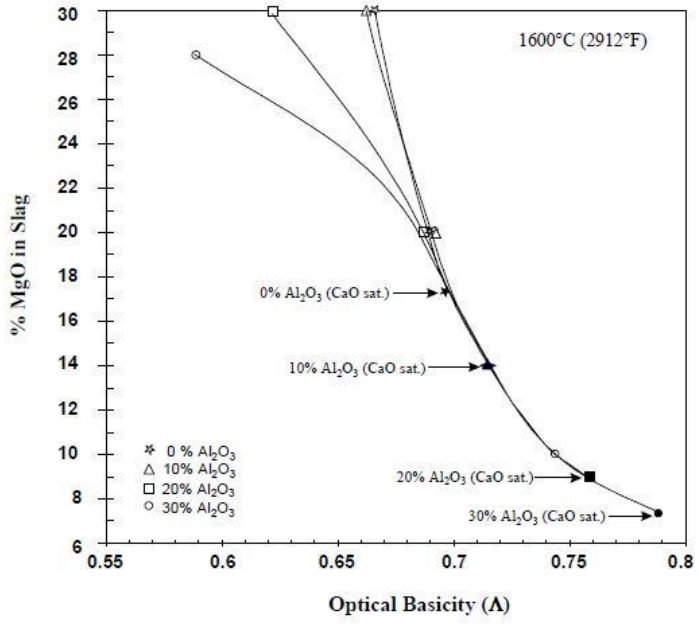

Figure 16: CaO-Al_2O_3-SiO_2-MgO at 1600◦C

Equation (9) can be used to calculate MgO solubility for the CaO-SiO_2-Al_2O_3-MgO system[16].

$$\%MgO = 1330.5\,\Lambda^2 - 2092\Lambda + 829.9 \qquad (9)$$

where 'Λ' is the calculated optical basicity

Equation (9) was derived using regression techniques for this particular slag system and was based on Eugene's work on ladle refining principles[16].

3.2.3 Determination of sulfide capacity

Sulfide capacity can be calculated using its correlation with optical basicity as stated in section 2.3.3, Equation (5)

$$\text{Log } C_s = \frac{[22690-(54640*\Lambda)]}{T} + [(43.6 * \Lambda) - 25.2]$$

An alternative correlations that was not based on optical basicity were available, but calculating optical basicity through slag analysis and using Equation (5) to calculate

sulfide capacity proved simpler and could be used for a wide range of slag compositions[33].

Equilibrium sulfur content in the steel was calculated using the sulfur distribution ratio result in Equations (6) and (7) defined earlier.

$$\log L_s = \log \frac{(\%S)}{[\%S]} = \frac{-935}{T} + 1.375 + \log C_s + \log f_s - \log a_o$$

$$[\%S^{eq}] = \frac{[\%S] * W_m}{W_m + L_s * Wslag}$$

3.2.4 Determination of lime required for desulfurization

The developed slag model calculates %CaO required by addition of lime/dolomite as a source iteratively until the required target level of sulfur is achieved. The amount of lime/dolomite added in weight (lbs) for every iteration and wt% CaO that enters the slag can be specified as input to the model calculation. The difference in wt% of CaO after the desulfurization and wt% CaO during the slag analysis provides the approximate amount of lime required for the desulfurization process.

Practically, changing the composition of the slag through addition of oxides changes the optical basicity value. Hence, it is very important to consider the newer composition for calculation of optical basicity and its effect on the MgO saturation level.

3.2.5 Recalculation of MgO

The slag model considers the number of iterations performed for lime calculation during the desulfurization and the change in wt% chemical composition of the slag. These updates are used to recalculate optical basicity and minimum wt% of MgO required for the slag to protect the refractory.

The model also calculates the weight (lbs) of magnesia or dolomite that should be used to achieve the calculated minimum MgO saturation. The option of selecting one of the sources for MgO either magnesia or dolomitic lime is also included in the slag model.

Another option was provided in the slag model software to view the calculated results plotted on the phase diagram of the system CaO-MgO-SiO_2. The use of a CaO-SiO_2-MgO phase diagram may not be very useful for ladle refining as the calculation depends on the degree of other components present in the slag, but this output can help to predict the liquid portion of the slag having CaO dissolved in it, and can be a helpful tool to design different types of slags. There were several situations where the CaO-SiO_2-MgO phase diagram plot was not accurate enough based on the calculations and was not usable due to the presence of other fluxes such as Al_2O_3 and CaF_2. This situation may arise if the $\%Al_2O_3$ in the slag is more than 5-25% in content.

3.3 Flow diagram

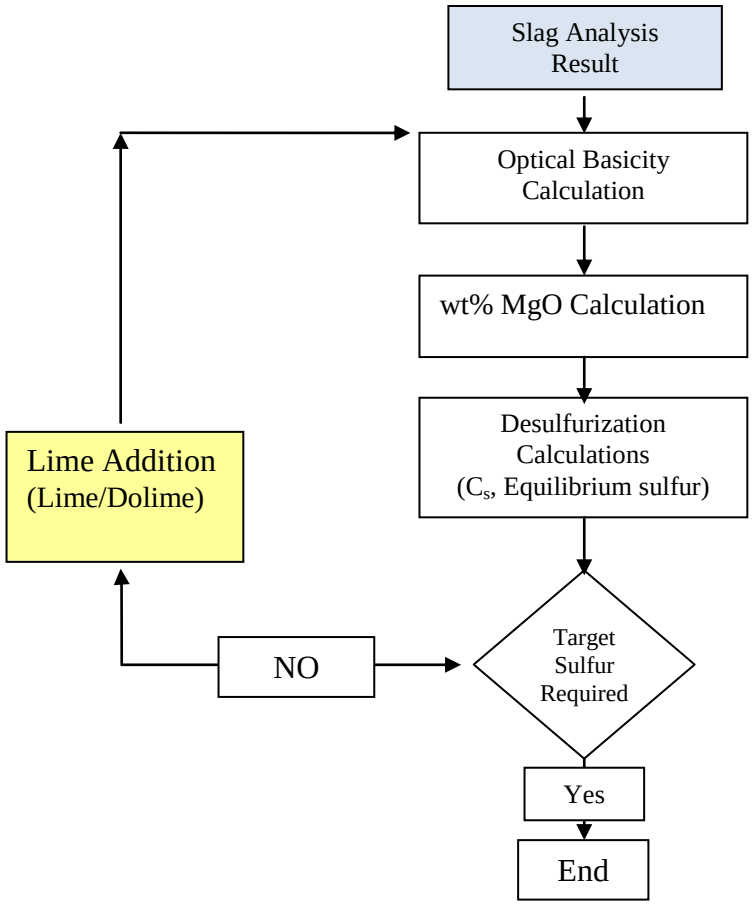

Figure 17: Flow diagram of slag model

3.4 Analysis procedure and techniques

3.4.1 Temperature

The temperature of the molten steel is measured in the ladle furnace with the aid of a temperature sensor probe. The frequency of taking the temperature is determined by the temperature control system.

3.4.2 Chemical composition analysis of steel

Similar to the temperature measurements, the operator takes the samples and sends them for inspection. The results of the chemical analysis automatically reach the ladle furnace operator screen. The samples are analyzed for the concentration of Al, Cr, Mn, Si, P, Mo, V, Ca, Ti, Mg and other minor elements.

3.4.3 Slag Analysis

EAF slag samples at Arcelormittal are analyzed through an ARL OPTIM'X WD-XRF Spectrometer. It is an advanced X-ray fluorescence sequential spectrometer which has the ability to precisely analyze for up to 90 elements. The concentration in percent weight of CaO, Al_2O_3, SiO_2, MgO, MnO, TiO_2, Cr_2O_3 and other oxides in minor concentration can be measured.

The slag analyzer available at Arcelormittal was not calibrated to analyze the ladle slag and required addition modifications. The slags were hence sent to Magnesita for analysis. Magnesita is a well known refractory brick manufacturer and they provide refractory bricks to Arcelormittal. The slag analysis results were then compared to model predictions.

Chapter 4 : Results and discussion

4.1 Theoretical Correlation

The slag model was used to evaluate different slags containing Al_2O_3 to see the effect on MgO saturation. Slags containing CaF_2 were also evaluated to compare MgO saturation behavior with theoretical results.

The following composition represents a slag sample from the ladle furnace of the system CaO-Al_2O_3-SiO_2-MgO at 1600 °C. Slag 'A' is the slag to be evaluated and Slag B is the optimum slag with saturated MgO only. The MgO saturation level in slag B was calculated using the developed slag model. CaO calculation was not possible in this model and is restricted to use only for desulfurization calculation.

Table 4: Slag analysis

Slag A		**Slag B**	
%MgO	12	%MgO	11.8
%CaO	45	%CaO	45
%Al_2O_3	26	% Al2O3	26
%SiO_2	17	%SiO_2	17

The result shows that the slag A is slightly oversaturated with MgO. This slag can be compatible with magnesia refractory as it is already saturated with MgO, in this case the CaO and MgO requirements for slag A is zero.

Similar examples were considered with slags of lower Al_2O_3 0 to 15 % (Table.5) and were tested using developed slag model for its effect on MgO saturation level. It was noticed that slags from Al killed steels have low MgO solubility. This can be correlated to Figure 13 and 14 which explain the decrease in solubility of MgO and increase in CaO solubility as Al_2O_3 content increases in the slag[16].

Table 5: Slag in $CaO-Al_2O_3-SiO_2-MgO$ system at 1600° C

Slag A	Slag B	Slag C
%MgO 17.24	%MgO 16.52	%MgO 13.58
%CaO 45.5	%CaO 45	%CaO 48
$\%Al_2O$ 0	$\%Al_2O_3$ 5	$\%Al_2O_3$ 10
$\%SiO_2$ 37.26	$\%SiO_2$ 34	$\%SiO_2$ 29

Slag containing fluorspar shows a different phenomenon in the solubility of CaO and MgO. It was noticed that when the CaF_2 content in the slag increases, the MgO solubility increases[16]. Industrial slags usually have both CaF_2 and Al_2O_3, which may have different variability in MgO solubility. If the slags are not CaO or MgO saturated, then the effect of CaF_2 can lead to high solubility of manganese from the refractory line[16, 35].

Even if calcium fluoride (CaF_2) content is not added directly, the existence of CaF_2 in small amounts can be seen due to a small percentage of fluorine in the slag. It is considered that $\%CaF_2 = 2* \%F$[16, 42].

4.2 Comparison of industrial measured values and calculated values

4.2.1 MgO saturation calculation

To test the accuracy of the model, slag samples after tapping were collected for analysis. The slag analysis results were used as slag composition input to the model and were solved to calculate MgO saturation.

Some results shown in Table 6 demonstrated the calculated MgO saturation level for the analyzed slag. The four slags that were tested with the slag model showed that the slags on average were oversaturated with CaO. Also, for sample no. 32929, 32977, 32904 it was noted that the slags were slightly under saturated with MgO. Considering the fact that Arcelormittal uses a magnesia slag line, it is very important to saturate the slag with MgO due to the existence of CaF_2.

Table 6: MgO saturation level for analyzed slags

Sample	Grade	MgO	CaO	Fe_2O_3	Al_2O_3	SiO_2	Cr_2O_3	TiO_2	CaF_2	Optical Basicity	Calc. MgO
32868	1025	13.44	47.63	1.26	3.21	24.66	0.11	0.56	5.20	0.736	10.94
32929	GR400	7.14	54.92	0.46	2.79	24.14	0.04	0.60	5	0.753	9.02
32977	5160	7.92	56.16	0.52	2.95	21.05	0.15	0.76	4.80	0.768	7.99
32904	W400	9.34	49.14	1.74	3.31	23.63	0.10	0.83	4	0.741	10.33

Consider Figure 18 for the optical basicity versus MgO for the above calculation. It was clearly noticed that the percentage of required MgO decreases as the optical basicity increases.

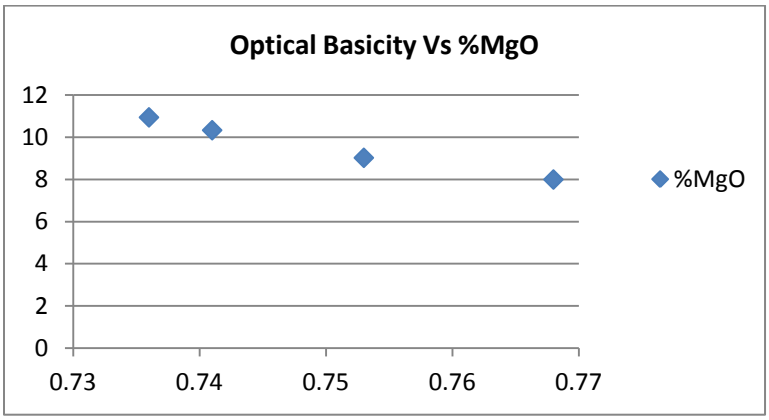

Figure 18: Optical basicity versus %MgO

A few more tests were conducted to test the MgO saturation calculations with the slag analysis carried out in year 2012. The analysis in Table 7 and Figure 19 show similar results and satisfy the optical basicity correlation.

Table 7: MgO saturation level for analyzed slags

Sample No.	%MgO	%CaO	Fe_2O_3	Al_2O_3	SiO_2	Cr_2O_3	TiO_2	CaF_2=F*2	Optical Basicity	Calc. %MgO
6312	10.25	51.12	1.01	2.12	23.87	0.11	0.38	5.8	0.747	9.60
6313	10.57	51.77	0.76	2.53	24.45	0.05	0.34	4.6	0.748	9.51
6314	10.75	49.77	0.44	2.68	25.79	0.06	0.43	5.6	0.737	10.73
6315	8.81	49.51	0.63	2.04	24.57	0.05	0.4	4.4	0.743	10.10
6318	11.22	47.58	1.3	3.37	25.62	0.17	0.54	5.4	0.731	11.68
6384	11.64	49.45	0.19	4.05	26.81	0.03	0.62	4.4	0.732	11.42
6386	11.24	50.95	0.43	3.79	23.4	0.08	0.68	4	0.748	9.46
6387	9.14	54.62	0.93	3.1	23.92	0.07	0.61	6.1	0.751	9.19

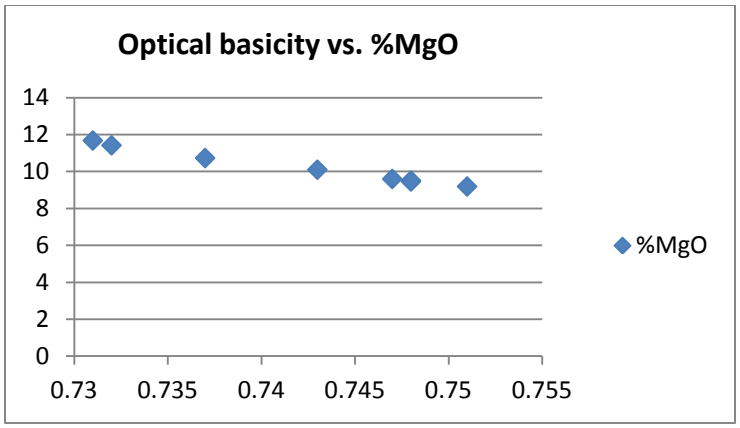

Figure 19: Optical basicity versus %MgO

4.2.2 Desulfurization calculation

The slag model was then tested for desulfurization calculation using analyzed slag data discussed in Table 7. The amount of lime required for target sulfur and %MgO required for the composition were calculated as shown in Table 8. The calculated results of lime required for desulfurization using the slag model were then compared with the industrial data. The slag model calculations showed good correlation with industrial data in most cases.

The following conditions were considered during the calculation. Metal weight-100 tons, slag weight – 200 lbs, oxygen content- 15 ppm and lime concentration of 98%.

Table 8: Desulfurization and CaO calculation

Sample	Grade	Optical Basicity	Calc. MgO	Initial Sulfur	Target Sulfur	Cs Sulfide Capacity	Lime Added	Calc. Lime	%MgO after Desulfurization
32868	1025	0.736	10.94	0.079	0.025	-2.46	104	119	7.66
32929	GR400	0.753	9.02	0.3	0.05	-2.22	246	250	8.46
32977	5160	0.768	7.99	0.5	0.025	-2.01	296	250	17.0
32904	W400	0.741	10.33	0.3	0.045	-2.40	1384	170	8.30

The first three results in Table 8 illustrate that the calculated amount of lime required is almost similar to the lime that was added during the ladle refining at the plant. Sample 32904 showed a huge difference in calculated lime and the lime that was actually added

during the ladle refining. This might have been due to the lack of data and operational variation for that particular heat.

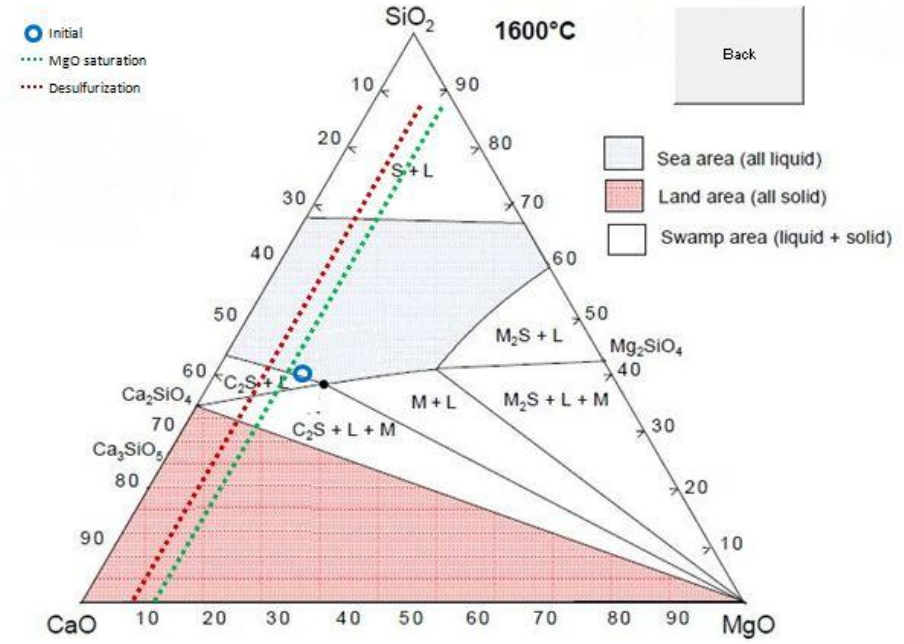

Figure 20 : Slag model calculation plotted in CaO-SiO_2-MgO slag system for sample # 32868

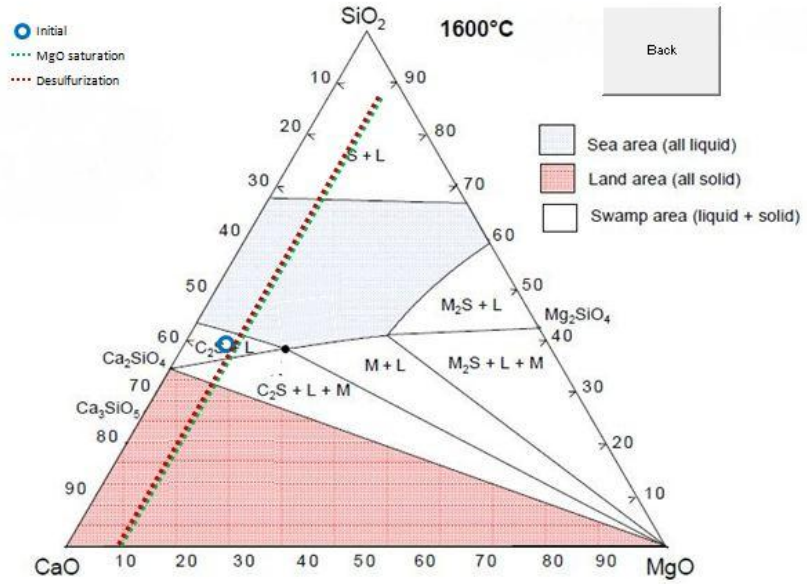

Figure 21: Slag model calculation plotted in CaO-SiO_2-MgO slag system for sample # 32929

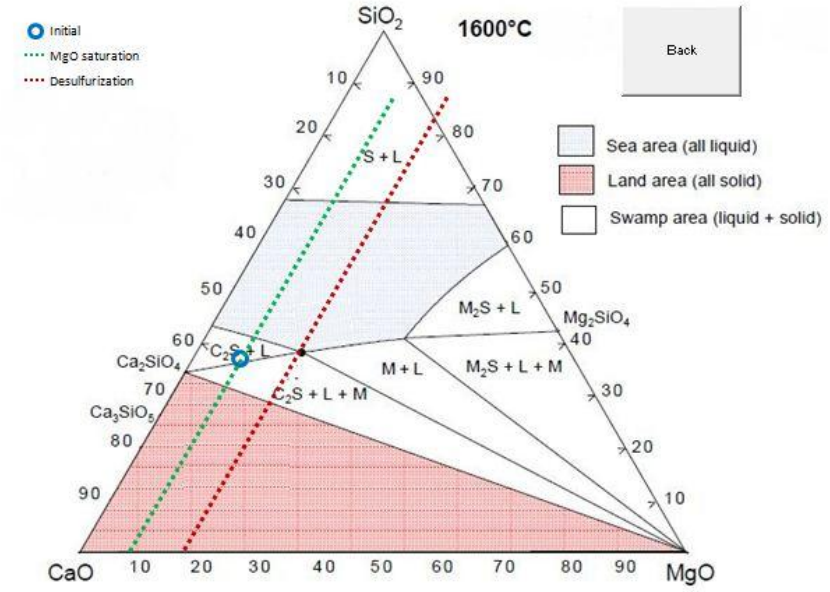

Figure 22: Slag model calculation plotted in CaO-SiO_2-MgO slag system for sample # 32977

Figures 20, 21, 22 show calculated results plotted on the phase diagrams of the CaO-SiO_2-MgO system.

4.2.3 Slag model limitations

The slag model has been designed to work with ladle slags and is applicable in the temperature range of 1600 to 1700 °C. Composition ranges for which the model gives best results are 0-30% MgO, < 0-5% Al_2O_3, and < 10% CaF_2. Content of Fe_2O_3 and Mn_2O_3 from the slag result should be reported as %FeO and %MnO in the slag model[33].

4.2.4 Discussion

Good agreement between the calculated and measured lime was obtained, as we can see in first three results in Table 8. MgO calculation and its correlation with optical basicity also proved to be correct for tested ladle slags. However, for prediction of CaO based on desulfurization, in some cases the calculated result was much less than the measured values as seen for sample # 32904 in Table 8. A probable reason for this might be either an error in the slag making process or an error in the scrap steel recipe. The

desulfurization and CaO calculation may also vary due to oxygen activity in the steel. In addition, the phenomenon of kinetics of desulfurization was not taken into account in the model, and it will be considered as a future development of the slag model.

Chapter 5 : Conclusion and Future Considerations

5.1 Conclusion

The first part of thesis has attempted to provide a detail understanding of slag making and slag quality control procedures. A slag model was developed to calculate the minimum %MgO required for better refractory life based on the slag analysis report and optical basicity calculations. Further, calculation of minimum CaO and MgO required after desulfurization of the steel was an additional option that was provided to verify the MgO saturation after the desulfurization process. The developed slag model can be a useful tool to design different types of slag for efficient operation at the ladle facility. If implemented with slag analysis devices in the process flow, this would prove to be a good on-line process control tool. In summary, the slag model gives reliable results for MgO saturation if the conditions are correctly specified. Proper measurement of oxygen activity, CaF_2, slag and metal weight are a few conditions which affect the calculation of MgO saturation. The slag model works well in the temperature range of 1500 to1700 ° C.

5.2 Future considerations

Future work should study more precisely the dependence of oxygen activity on the desulfurization and to integrate kinetics of desulfurization theory into the present slag model. This will make the tool more precise for desulfurization and CaO calculations. Another aim for future work would be to develop a model to predict dual saturated slags for dolomitic slag lines for which more precise CaO saturation calculation needs to be designed for the $CaO\text{-}SiO_2\text{-}MgO\text{-}Al_2O_3$ system.

Part 2- Caster Productivity

Chapter 1 Introduction

"Continuous casting or strand casting is the process whereby molten steel is solidified into semi-finished billet, bloom, or slab."[14]

Continuous casting is used to solidify around 1.5 billion tons of steel produced in the world every year[43]. Continuous casting has many advantages over other casting processes: lower capital costs, higher yield, improved quality of the cast product, lower operating costs, e.g., slabs are sent directly to hot rolling and do not require pits for reheating; thus, moulds and mould shops are eliminated.

Continuous casting is considered most efficient and economical when large heats are cast and when multiple casting strands are used. To achieve better productivity and operating conditions for these multiple casting strands, the process needs to be rigorous and sensitive. Many factors like tundish design, nozzle geometry, cooling water rate, mould cooling and design influence the casting process[44]. The most important factor in a continuous casting operation is to have control over strand cooling and shell growth along the machine. These have an extensive influence on the formation of cracks and other defects formed on the cast. Usual defects found are non-metallic inclusions, corner/radial cracks, transverse and longitudinal surface cracks.[44]. To have defect free castings, parameters like casting speed, machine design and product dimension have to be controlled for different steel grades. Continuous casting is essentially a heat extraction process where heat transfer plays a very important role in terms of quality and productivity. Thus, it has been very important for steelmakers to concentrate on heat transfer phenomena and liquid pool length to optimize casting speed for better productivity[45].

Considerable research has been carried out to understand and improve heat transfer for better operating conditions of a continuous caster. Studies included, nozzle design to control fluid flow, heat transfer calculations to predict the liquid pool length as a means

of establishing more proficient operating conditions, and structure of the metal and solidification profile to have control over quality.[44]. A few research results and theories which are of interest to this project are discussed in the literature review in Chapter 2.

1.1 Process description

In the continuous casting process, as shown in Figure 23, molten steel flows from a ladle through a tundish into the mould. The solidification of steel during the continuous casting process takes place in three stages: in the mould, in the secondary or water spray zone and in the air cooling zone.

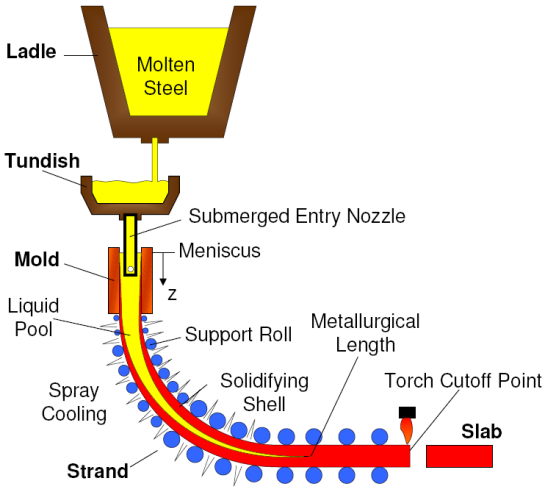

Figure 23: Schematic of continuous casting process[46]

Once the molten metal flows into the mould, a solid outer shell is formed due to high heat transfer between water cooled mould walls and the liquid steel. Periodic oscillation of the mould prevents sticking of the solidifying liquid steel to the mould walls. This process creates oscillation marks on the shell and they are the preliminary sites for generation of cracks. To avoid non-uniform initial solidification and surface defects, control of the liquid flow along the top surface of the mould and horizontal velocity which controls heat transfer in the liquid and solid flux layers are very important[46].

Initial solidification arises at the meniscus which is governed by conduction of heat through the mould, latent heat and liquid flux infiltration. After the initial rapid solidification in the mould, further solidification is governed by conduction and radiation across the gap between the mould and the steel shell. The air gap between the mould and the steel shell can be controlled by the amount of taper of the mould walls[46].

After the shell exits the mould and enters the spray zone, the steel billet is subjected to large surface temperature fluctuations which cause phase transformation and other micro-structural changes, which affects the quality of the steel. The steel billet with an outer shell and a liquid pool inside is withdrawn with the help of drive rolls, which also help the steel from bulging due to ferrostatic pressure. Due to friction against the rollers and ferrostatic pressure, the steel shell is subject to complex internal stress which causes defects and deformation[46]. Further, water spray and air mist sprays cool the surface of the strand between the rollers to maintain the surface temperature of the billet until the core is solid. Once the center is completely solid the strand can be torch cut to required lengths.

We shall concentrate on various mathematical models in further sections to investigate heat transfer phenomena as a function of controllable process parameters in order to achieve the objective of developing an empirical model at the continuous casting zone to increase the casting throughput.

Chapter 2 Literature Review

Continuous casting is a heat extraction process wherein solidification takes place in three stages: cooling in the mould, secondary water spray cooling and air cooling. The quality control system based on temperature sensing and control over process variables assists the process of continuous casting to reduce the cost of manufacturing and to have a better quality product. Important process parameters can be estimated using different theoretical models, and hence, mathematical models for heat transfer in continuous casting were developed to correlate the mechanical properties of the steel slab with process parameters to understand the effects of input variables on the temperature distribution[47].

Understanding the heat transfer during solidification and at the solid-liquid interface to satisfy laws of conservation of heat, mass, force, boundary conditions phenomenon is necessary to control the continuous casting process to ensure defect free products. Also, control over the liquid pool length is a key element in optimizing the casting speed with respect to a good level of productivity[48].

Complexities like unknown position of the phase change boundary, change in density during the solidification, determination of convective and radiative heat transfer coefficients or heat fluxes, and mathematical modeling of the heat transfer problem and temperature distribution throughout the strand is very challenging[49].

Due to the above mentioned complexity and nonlinearities it is very difficult to obtain analytical solutions for the problem[49], but numerical techniques like finite difference, finite element and boundary element are capable of solving mathematical models of the heat transfer, wherein the equations are descretized using the above mentioned techniques. Moreover, mathematical models, once verified, are easy to use and comprehensive in simulating the thermal state of the cast[49].

2.1 Mould heat transfer

In continuous casting processes, the mould is the most complex and critical part, which controls initial solidification and surface quality. Heat transfer in the mould zone is primarily controlled by heat conduction between the mould and the solidifying shell, radiation through the mould strand gap and convection by the cooling water. The size of the gap between the solidifying shell and the mould wall is constantly changing in response to dynamic conditions of the mould. Thus, the variables that affect the dynamics and properties of the air gap have an impact on the heat transfer in the mould[50].

The heat transfer characteristics in the mould in response to different casting conditions were studied, where operating parameters like casting speed, carbon content superheat, cooling water amount and billet size were considered for the study. In one of the studies on continuous slab casting by M. Makinen and M. Uoti[51], mould plate temperatures in the steady state were compared between different locations in the mould by varying operating parameters. The research concluded that, increasing casting speed increases average temperature in the mould. This is due to more liquid metal entering into the mould and reduced thickness of the strand. It was also noted that there was a 20% increase in liquid pool depth (depth of molten metal inside the solidifying shell) when the casting speed was increased by 15% [51]. Oscillation of the mould has been noted to influence to the surface quality of the slab wherein increasing the oscillation frequency decreased the depth of surface marks[51].

According to previous studies it was found that increasing the casting speed causes the average mould heat transfer to increase at the midfaces and mould corners[50]. C. Chow and I.V. Samarasekera during their study on the effect of casting speed on temperature distribution noted that there is high heat transfer at higher casting speed. The reason for this is the thinner shell, which reduces mould–strand gap and improves mould–strand contact; also, the hotter billet surface temperature drives more heat flow[50]. Studies found that for casting speeds up to 1.3 m/min (meters per minute) the heat transfer was found to be 3100-3500 kW/m^2 for low carbon grades[50, 52]. The result also demonstrated that the effect of casting speed on mould heat transfer was also influenced

by carbon content and it was found that for higher carbon content, a change in casting speed resulted great change for the average mould heat transfer. Refer to Figure 24[50]. Also, the effect of carbon content on the mid-face mould heat transfer was published as in Figure 25[50].

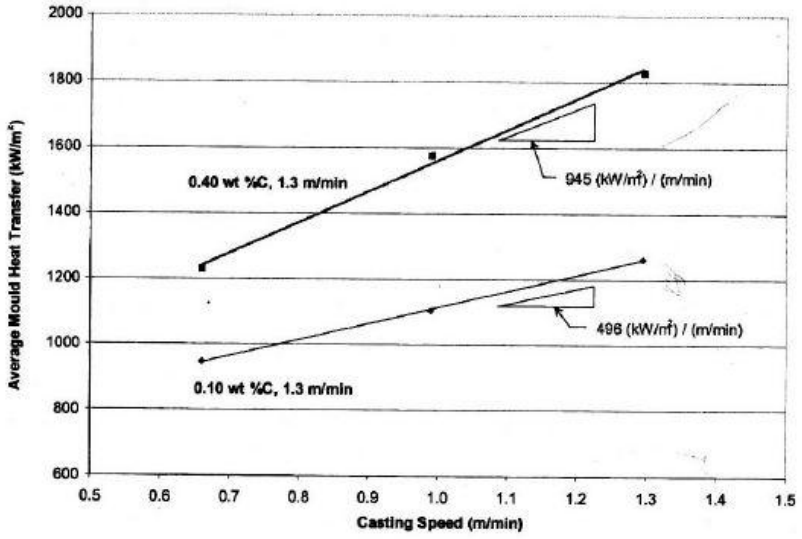

Figure 24: Average mould heat transfer versus casting speed[50]

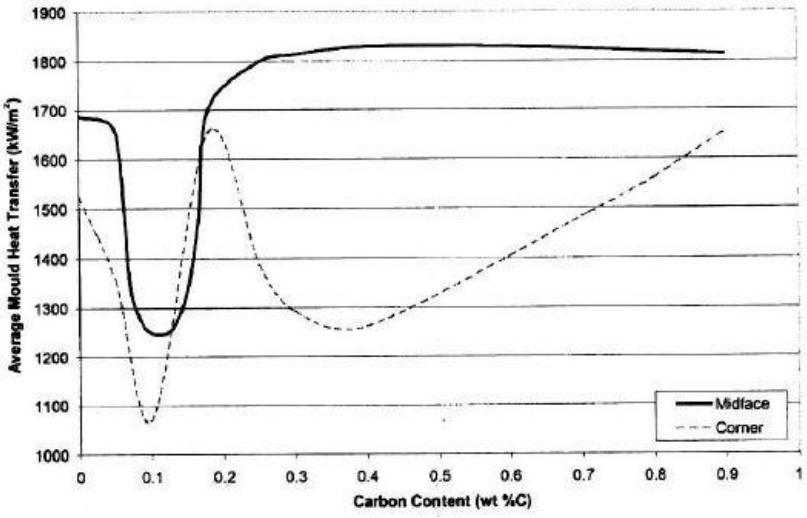

Figure 25: Average heat transfer versus carbon content[50]

The effect of water flow rate on mould heat transfer was noted to have very little impact on the heat transfer in the system, but a minimum water flow rate of 10–12 m/s (meters per second) has to be considered for uniform and sufficient cooling[50].

Secondary cooling is also a critical part of the continuous casting process. Secondary cooling can influence billet quality. Secondary cooling is used to extract heat and promote solidification of the liquid inside the strand. The rate of solidification is increased by spraying water or a combination of air and water[14].

2.2 Secondary cooling

Conduction, convection and radiation are the basic forms of heat transfer that can be defined in this zone. All three forms of heat transfer can be described by the following equations at various sections of the cooling zone. Radiation occurs in the upper region of the secondary cooling zone and at the air cooling zone where heat is transferred from the outer surface of the cast section to the ambient[14]**.** Convection is the primary form of heat transfer in the secondary cooling zone.

Radiation: $$Q = \sigma E A (T_s^4 - T_a^4)$$

where σ is the Stefan-Boltzmann constant, E is the emissivity, A is the surface area, T_s and T_a are steel surface and ambient temperatures[14].

Conduction: $$Q = k\ A\ (T_i - T_o)/\Delta X$$

where k is the thermal conductivity of the steel, A is the cross sectional area, and T_i and T_o are the shell's inner and outer surface temperature respectively[14]. $T_o = T_s$ in the radiation and convection equations.

Convection: $$q = h\ A\ (T_s - T_w)$$

where h is the coefficient of heat transfer, A is surface area, T_s and T_w are the steel surface and spray water temperatures respectively[14].

In Jaroslav and Miroslav's paper on secondary cooling of continuous casting [53], a new generation of mist nozzles was tested for a wide range of water and air pressure combinations. Experimental methods for measurement of heat transfer parameters of nozzles for various casting speed were suggested. Different analysis techniques like PDA (Phase Doppler Anemometry) were used to find valuable results showing important aspects for secondary cooling design and control[53].

Internal and external cracks are normally observed defects due to improper secondary cooling and excessive heat extraction rate[54]. Study of the secondary cooling design by using the optimization Broydon-Fletcher-Goldfarb-Shanno (BFGS) method was carried out by determining constant heat transfer coefficients in spray zones. An optimization model used in this model gave good predictions for better cooling in the secondary cooling zones. Results also showed that slight variation in the casting speed and other parameters could change the cooling pattern in the spray zone considerably[54].

Similarly, solidification heat transfer in mould and other regions has been broadly studied and many articles on the subject are published in academic and industrial fields. Computational 2-dimensional and 3-dimensional heat transfer models have been developed since the realization that computer simulation can solve critical process models. Pehlke published his first paper describing computer modeling of continuous casting, and continued his work on computer application in metallurgy and developed a model which considered heat transfer in both mold and secondary cooling zones[55, 56].

Air gap formation in the mould and heat flow in the continuous slab casting was theoretically studied using a mathematical model. Brimacombe et al. in their investigation to predict casting conditions to achieve defect free casting and to avoid break-outs found that hot spots can form on the surface of the slab which may lead to defects. The behavior of the gap and heat flow to varying casting speed, slab dimensions and mould taper were also studied[57]. It has been shown that the shape of the gap can have an effect on the presence of hot spots on the surface of the slab causing break-outs and defects[57].

Richard A. Hardin et al. assumed a two dimensional transient simulation model to control the slab caster. Slab solidification conditions were computed by the model as a function of varying casting speed, spray cooling water flow rates, and slab dimensions[58]. The Dynamic Spray Cooling Simulator (DYSCOS) computer program developed at IPSCO Inc. (Prairie Pipe Manufacturing Co., Ltd) was used to simulate transient caster operation. This offline model was able to run in two modes, transient simulation mode and control mode. In transient simulation mode, the casting speed, water flow rates and other operating conditions was defined and were time varying. Based on these operating conditions, temperature and solidification conditions throughout the slab were computed[58]. The comparison with measured surface temperature showed that the predictions were within ± 30 °C of the measurements for the transient model[58]. The DYSCOS model was an accurate simulator and was useful in developing control methods which maintain slab surface temperatures within desired ranges[58]. Tieu and Kim [47] developed a computational three dimensional unsteady heat transfer model to calculate the temperature distribution and solid shell thickness profile of a continuous cast slab. The model considered non-linear material properties of specific heat and thermal conductivity and phase change phenomenon during solidification. PHOENICS [59], a general thermo-fluid mechanics computer program developed by CHAM(Concentration, Heat and Momentum Limited) was used to solve the heat transfer equations. The calculated thermal profiles and solid shell thickness were in good relation to those predicted by an industrial model and experimental measurements[47]. Panagiotis [60] in his work on modeling of the solidification phenomena for slab casters belonging to the SIDENOR group of companies considered a three dimensional numerical solution of the differential equation of heat transfer. The model also considered strain analysis and solid fraction analysis, which helped the model to predict internal defects. The results showed that solidification was almost constant along the length of the billet after it leaves the caster. It was also noted that the higher the carbon content of the slab, the more it takes to solidify downstream. Furthermore, it was stated that the higher casting speed would take more time to complete solidification[60].

Many offline mathematical models were developed with interesting findings which motivated further development of an on-line application to control the casting process and to optimize casting speed. Louhenkilpi et al. developed a real-time heat transfer model for continuous slab casting which calculated strand temperature and solid shell thickness profiles along the strand length as a function of casting variables[45]. The model was two-dimensional where the heat flow along the width direction of the strand was neglected. Another assumption was that the solidus and liquidus temperatures and other phase transformation temperatures were considered to be constant. Accuracy of the model was tested by comparing simulation data with surface temperature measured using pyrometers. Multiple trials were taken by keeping casting speed constant and varying the water flow rates and vice versa. It was noted that the model gave reliable results with very few errors. The model also fulfilled the speed requirement concerning its on-line use. Also, a special procedure to determine the heat transfer coefficients and other boundary conditions based on water flow rates and casting speed was developed successfully[45].

Another two-dimensional slice model with nonlinear thermodynamics and transport properties was developed to calculate the bloom surface temperature, liquid core temperature, solid shell thickness profile along the strand and solid fraction[61]. The difference between the calculated surface temperature by the developed software and the measured surface temperature was less than 35°C with relative error lower than 3.5%[61]. Through a finite difference model programmed in visual C++, the temperature distribution of the bloom was simulated and optimum process requirements were met which improved casting quality[61].

Break-out is a serious issue in steel billet manufacturing as the molten steel that escapes through the solid shell usually runs onto the floor causing stoppage of the casting operation and can lead to heavy losses[57]. Hence, understanding the causes of break-outs and measures to increase the casting speed is fundamentally important for efficient operation of the caster. Heat transfer analysis in the mould and secondary cooling zones has to be considered before any changes in casting speed. The real time or online models should be supported by efficient mould design and water cooling rate[57].

2.3 Objectives of the present work

In this part of the thesis, the modeling of the temperature distribution along the strand length for the billet caster at Arcelormittal Contrecoeur West is presented. The research task is to develop a model that allows increasing the casting throughput to a safe limit such that there are no surface defects on the billet and liquid metal does not leak out when the end of the billet is cut. Systematic measurements of the steel billet surface temperature using a pyrometer at several points during the casting process provided data to create a model of the heat transfer during the cooling of the billet. A stationary non-isothermal flow and general heat transfer simulation model was developed using Comsol Multiphysics 4.2 software. The simulation results and plant trial results were then compared to analyze the error and to predict the inner temperature profile of the steel billet based on the measured surface temperature. The outcome of the analysis was used to boost the productivity of steel billet production within a safety limit. The methodology was applied to two carbon steel grades 1025 and 5160. Experimental setup and model formulas that bind the non-isothermal flow and heat transfer with the various solidification parameters and results are presented and discussed below.

Chapter 3 : Set up and experiments

Pyrometer measurements are currently considered the most reliable and cheapest way to measure the temperatures of cooling metal. Surface temperature measurement during the continuous casting process is a challenge due to an unsafe operational environment. Thus, pyrometers can be well utilized in these situations to have reliable temperature data.

To achieve the objective of building a reliable heat transfer model and to increase the productivity of the caster, work was started by taking temperature measurements at Arcelormittal Contrecoeur. Systematic surface temperature measurement at several points during the casting process for a sufficient number of distinct process instances was necessary for the grades of steel that were considered for the tests. Two grades of steel were considered, a low carbon steel grade 1025 and high carbon steel grade 5160H. The

carbon content of the other grades manufactured by Arcelormittal Contrecoeur was between these two grades.

The industrial trial was carried out with a four strand curved billet casting machine with a radius of 26 feet. Side view of the caster strand at Arcelormittal is shown in Figure 26.

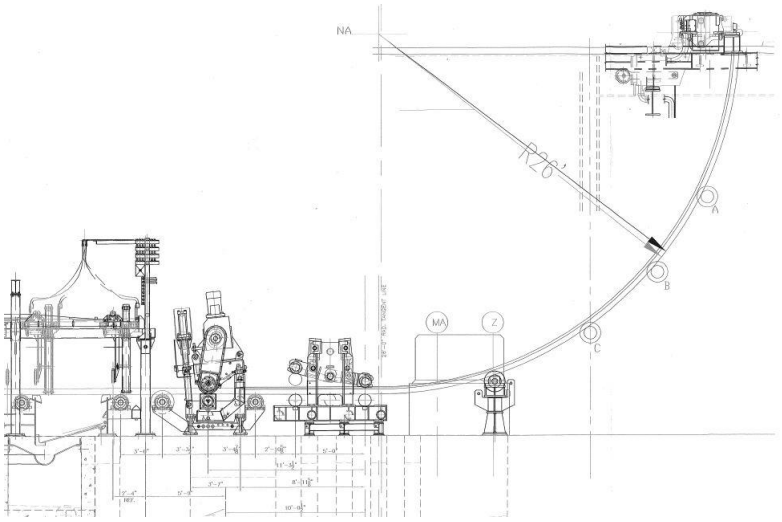

Figure 26: Side view of caster strand at Arcelormittal

Multiple zones were selected for the measurements, and arrangements were made accordingly to take the trials. A Modline 52 series pyrometer was used for the trials with a temperature range of 500 to 3000 °C and spectral range of 0.85-1.1µm. The Modline 52 series pyrometer has high resolution optics with adjustable focus to enable precise targeting.

Six trials were conducted totally out of which four were for grade 1025 and two for grade 5160. Due to the complexity of the casting equipment and the high heat, the trials were conducted only after the secondary cooling zone far below the mould. The pyrometer was not made to be used in zones with steam and other fumes, which hampered the accuracy of the instrument. Several zones were selected for the trials as shown in Figure 27 with the pyrometer focused perpendicular to the top surface of the steel billet.

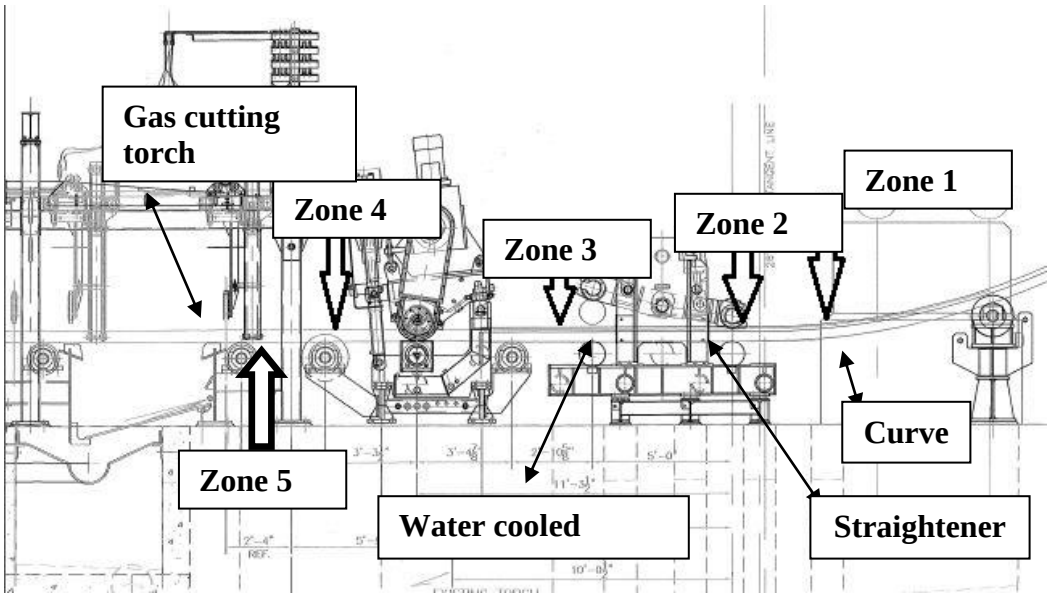

Figure 27: Selected zones for measurements

Approximately 23 feet of casting strand length between the caster exit and the gas cutting torch were selected for the temperature measurements. Figure 27 illustrates temperature measurement zones and positions of the rollers, straightener and gas cutting torch. The gas cutting torch (left section of the Figure 27) was used as a reference point, and the distances of the Zones 1 to 4 was measured from the reference point. Zone 1 is the curved section of the casting strand from where the solidifying billet starts to straighten. Zone 2 represents positions of a straightener where the billet is straightened.

Distance of the measurement zones from the gas cutting torch were measured to be as in Table 9.

Table 9: Distances of temperature measurement zones from the gas cutting torch

Zone	**Distance from the torch**
Zone 1	Around 23 feet
Zone 2	19 feet
Zone3	13 feet
Zone 4	6 feet
Zone 5	3-2 feet

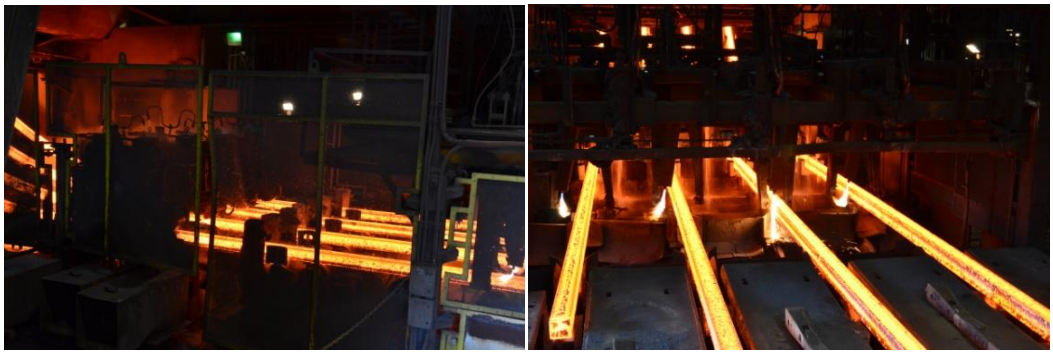

Figure 28: Side view of the strand and view of gas cutting torch at Arcelormittal

Pyrometer measurements were found to be very noisy due to the scaling on the billet and due to the steam produced near the water cooled rollers. In some cases an average temperature was considered as the fluctuation was very high during the measurements. An example of pyrometer measurements during a casting trial for 1025 steel grade taken at Zone 1(Curve) is shown in Figure 29. This example refers to the temperature measurement fluctuation due to operational variation and scaling on the billet. Reasons and explanation to these effects is described in Chapter 4 (Results and Discussion).

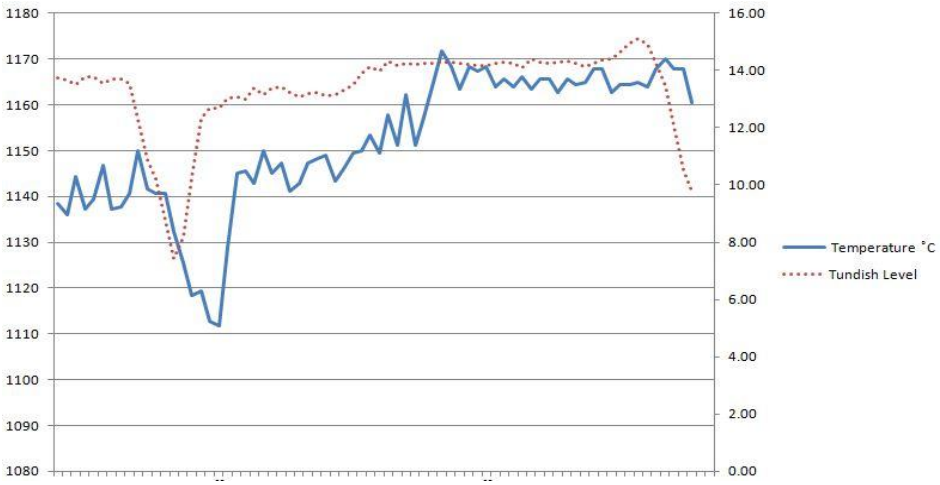

Figure 29: Sample showing temperature profile using pyrometer at zone 1

The data measurement and the simulation analysis using Comsol software were to find the optimum casting speed and then apply the findings to the industrial process. The considerations for building the non-isothermal fluid heat transfer model are discussed in

detail with simulation results showing temperature distributions across the strand. The calculated temperatures at the center and surface of the billet are compared with measured surface temperatures to find the fastest, yet safe, speed of the casting considering all the error factors.

Chapter 4 : Model formulation

A mathematical model that includes phase transformation phenomenon and that is based on the previous research efforts [61, 62] was built to predict the temperature distribution during solidification in steady state.

Comsol Multiphysics version 4.2 was used as a simulation tool to model the heat transfer problem which also included phase change phenomenon in terms of the release of latent heat. The model is based on original work by J. Fjellstedt [63]. The fluid flow non-isothermal heat transfer module in the Comsol software was used to define a stationary steady state process where the heat transfer equation is defined as[64]:

$$\rho C_p \boldsymbol{u}.\nabla \mathbf{T} = \nabla.(\mathbf{k}\nabla \mathbf{T}) + \mathbf{Q} \qquad (10)$$

where k is the thermal conductivity, C_p is the specific heat, Q is the heat transfer rate per unit volume and ∇T is the change in the temperature[64].

The 2D axisymmetric non-isothermal heat transfer model is identical to the incompressible Navier-stokes application with extra terms in the equation. The modified equation is designed to consider the changes in the density, enthalpy and specific heat capacity of the liquid metal[64]. Thus, the equation for 2D axisymmetric section with laminar flow using non- isothermal flow interface can be stated as[64]:

$$\rho \frac{\partial \boldsymbol{u}}{\partial t} + \rho(\boldsymbol{u}.\nabla)\boldsymbol{u} = \nabla.\left[-p\mathbf{I} + \eta(\nabla \boldsymbol{u} + (\nabla \boldsymbol{u})^T) - \left(\frac{2\eta}{3} - \kappa\right)(\nabla.\boldsymbol{u})\mathbf{I}\right] + \boldsymbol{F}\frac{\partial \rho}{\partial t} + \nabla.(\rho \boldsymbol{u}) = \mathbf{0} \qquad (11)$$

where

- η is the dynamic viscosity
- κ is the dilatational viscosity
- ρ is the density
- u is the velocity field
- p is the pressure
- F is a volume force field such as gravity.

Volume Force: The volume force vector, F= (F_X, F_Y, F_Z), describes a force field. Unit is force/volume.

A simple 2D geometry designed in Comsol is considered for simulation as shown in Figure 30. Various boundary conditions are applied at different sections representing mould, secondary cooling and air cooling zones.

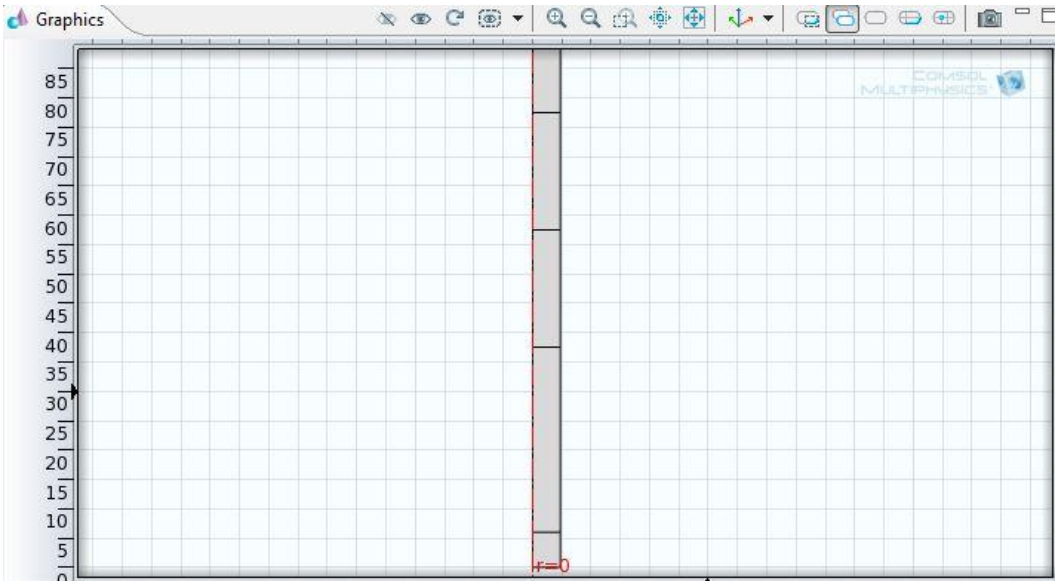

Figure 30: 2D section of the billet along the axis ‘r’

4.1 Boundary conditions

The following initial and boundary conditions were employed in order to solve the heat transfer equations.

- The temperature T was considered to be equal to the incoming liquid temperature,

$$T=T_0$$

- Heat transfer between the cast section and the mould cooling water and convective cooling is governed by Equation (12):

$$-\boldsymbol{n}.(-\boldsymbol{\kappa}\boldsymbol{\nabla}\boldsymbol{T}) = \in \boldsymbol{\sigma}(\boldsymbol{T}_{\boldsymbol{ext}} - \boldsymbol{T}) \tag{12}$$

  where T_{ext} is the external temperature.

- Radiation for surface to ambient is given by:

$$-\boldsymbol{n}.(-\boldsymbol{\kappa}\boldsymbol{\nabla}\boldsymbol{T}) = \boldsymbol{\epsilon}\boldsymbol{\sigma}(\boldsymbol{T}_{\boldsymbol{amb}}^{\boldsymbol{4}} - \boldsymbol{T4}) \tag{13}$$

  where T_{amb} is the ambient temperature.

- The equation at the inlet section of the stationary process with pressure and no viscous stress is given by Equation (14),

$$\boldsymbol{p} = \boldsymbol{p}_{\boldsymbol{0}}, \left[\boldsymbol{\mu}\left(\boldsymbol{\nabla}\mathbf{u} + (\boldsymbol{\nabla}\mathbf{u})^{\mathrm{T}}\right) - \frac{\mathbf{2}}{\mathbf{3}}\boldsymbol{\mu}(\boldsymbol{\nabla}.\mathbf{u})\mathbf{I}\right]\mathbf{n} = \mathbf{0} \tag{14}$$

  where p is the pressure.

The casting speed ‘u’ along the z direction is modeled, thermal conductivity is constant throughout the strand at all phases, the surface of the billet is cooled equally, latent heat evolved at solidification is accounted for by adding it to the specific heat based on the temperature.

4.2 Simulation

Thermo-physical properties of the metal grades 1025 and 5160, such as thermal conductivity, specific heat, density, latent heat, volume force (F), necessary for the simulation were taken from literature data [56, 65-68].

Defined material properties and casting parameters considered for simulation are as shown in Tables 10-12.

Table 10 Material properties supplied for simulation

Material properties defined for grades 1025 and 5160
Density
Dynamic viscosity
Thermal conductivity
Heat Capacity at Constant pressure
Ratio of specific Heat

Table 11: Casting parameters for grade 1025

Description(Grade 1025)	**Values**
Density	7858 (kg/m^3)
Thermal conductivity (k)	51.9 [W/(m*K)]
Dynamic viscosity μ	0.0434 (Pa*s)
Ratio of specific heats (gamma)	1
Ambient temperature (T0)	300[K]
Steel inlet temperature (T_in)	1828[K]
Casting speed (v_cast)	50.8[mm/s]
Melting temperature (T_m)	1678[k]
Enthalpy (dH)	205[kJ/kg]
Volume force damping constant (ε)	1e-3
Surface emissivity, air exposure	0.8
Heat transfer coefficient, mold (h_mold)	800[W/(m^2*K)]
Heat transfer coefficient, air (h_air)	10[W/(m^2*K)]

Table 12: Casting parameters for grade 5160

Description(Grade 5160)	**Values**
Density	8000 (kg/m^3)
Thermal conductivity (k)	42.7[W/(m*K)]
Dynamic viscosity μ	0.0434 (Pa*s)
Ratio of specific heats (gamma)	1
Ambient temperature (T0)	300[K]
Steel inlet temperature (T_in)	1828[K]
Casting speed (v_cast)	50.8[mm/s]
Melting temperature (T_m)	1648[k]
Enthalpy (dH)	205[kJ/kg]
Volume force damping constant (ε)	1e-3
Surface emissivity, air exposure	0.8
Heat transfer coefficient, mold (h_mold)	800[W/(m^2*K)]
Heat transfer coefficient, air (h_air)	10[W/(m^2*K)]

The relevant casting machine specification and operating conditions were as listed in Table 13:

Table 13: Casting machine specification

Main Design	**Parameter**
Machine type	Curved, 26 Feet Radius
Mould Material	Copper
Mould Length	0.8 meter
Mould Lubrication	Oil
Total Strand length	62 Feet
Pyrometer Distance from target	10 Feet

Two types of steels were casted during the plant trials listed in Table 14 with composition.

Table 14: Steel composition of grades selected during the trial (in mass %)

Grade	C	Si	Mn	P	S	Al	Cu	Ni	Cr	V	Mo
1025	0.27	0.25	0.90	0.025	0.025	0.004	0.8	0.3	0.250	0.005	0.08
5160	0.61	0.35	0.80	0.020	0.025	0.004	0.3	0.2	0.8	0.06	0.06

Chapter 5 : Results and discussion

There were few operational variations that affected the temperature measurement during the trials. From Figures 31 and 32, the effect of tundish level variation and casting speed variation on the surface temperature can be noticed.

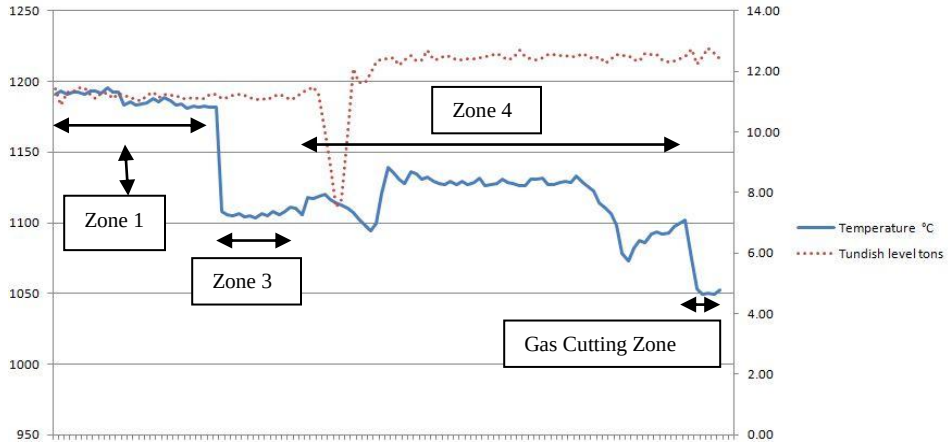

Figure 31: Surface temperature versus tundish level variation

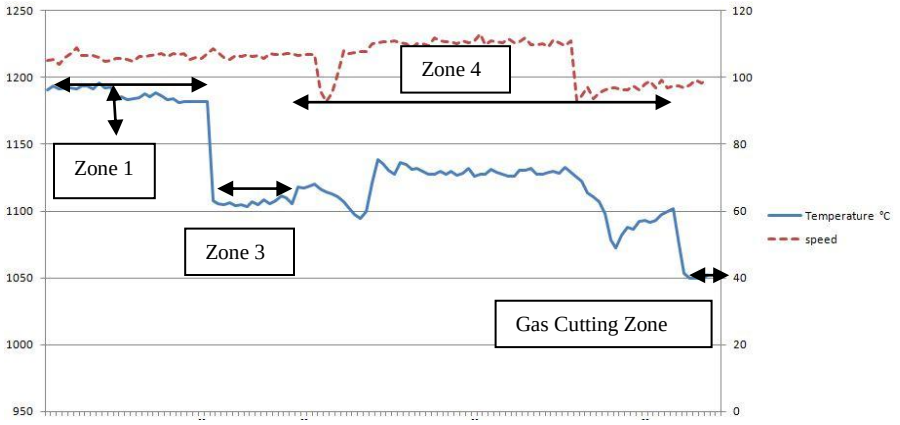

Figure 32: Surface temperature versus casting speed variation

5.1 Effect of tundish level fluctuation:

The speed of the caster is based on the liquid level in the tundish and is continuously adjusted at Arcelormittal Contrecoeur. Casting speed is decreased as the liquid level in the tundish is reduced to match the refilling process of the tundish. This is essential to keep the process continuous and to avoid stoppage of the caster.

The variation in speed due to the liquid level in the tundish had an effect on the temperature measurements that were taken during the trials. In Figure 31, a considerable drop in temperature in the Zone 4 section of the graph is noticed. This effect is due to two main reasons: 1. very low temperature of the liquid steel in the tundish. 2. low casting speed which helps the solidifying billet to transfer more heat in the mould and secondary cooling zone. The variation in speed and its effect on temperature measurement can be noticed in Figure 32. The casting speed profiles follow the metal level signals quite closely with a small time lag, which is reflected by the measured surface temperatures. These effects were important and were considered during the comparison with simulation result. Multiple simulations were run at different casting speeds to have a good comparison based on the different zones where the measurements were made.

The accuracy of the heat transfer model was tested by comparing surface temperatures measured using a pyrometer and obtained by the simulation model. Few results showing the surface temperatures calculated by the model and measured by the pyrometer are shown in Figures 33 and 34 for the grade 1025 (low carbon). The pyrometer data were noted every second throughout the trial and later the data were refined accordingly. The fluctuations due to scaling on the surface of the billet had to be neglected in a few trails, in which only the higher temperature data were considered for the comparison.

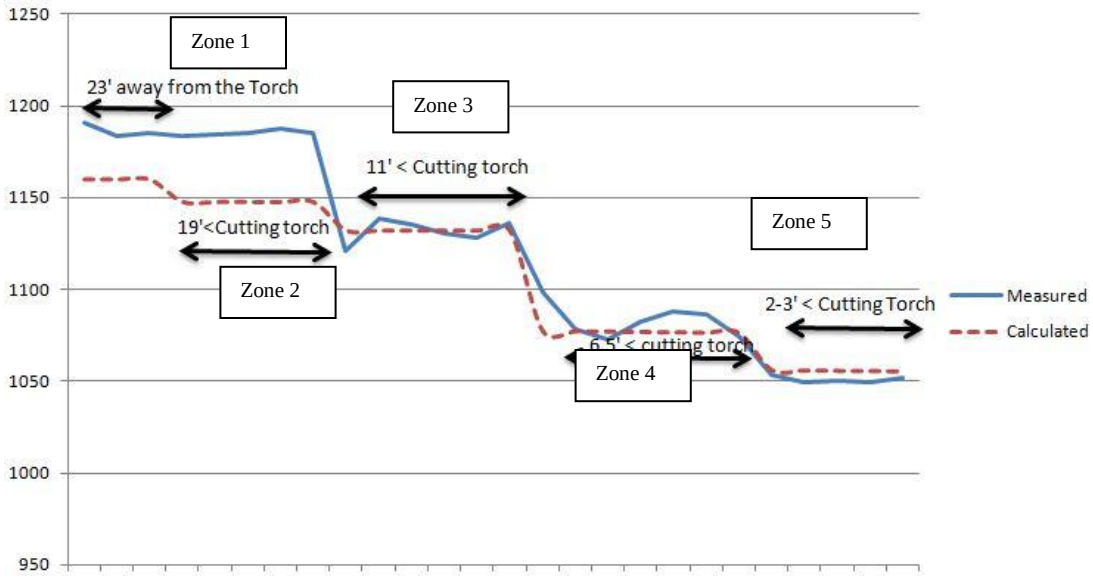

Figure 33: Measured versus calculated surface temperature for grade 1025 Trial 1

In Figure 33, the arrow section represents the zones where the pyrometer measurements were taken. Zone 1, extreme left of the graph lays approximately 23’ before the gas cutting torch, zone 2- 19’ before the torch, zone 3 - 11’ before the torch, zone 4 - 6’ to 6.5’ before the torch, zone 5 - 3’to 2’ before the torch. The temperature in zone 1 (23’ before the cutting torch) near the lower curved section of the strand was measured at a casting speed of 105 inches/min. The speed gradually decreases towards the end zone 5 to around 95 inches/min. This change was due to the reducing liquid level in the tundish. Multiple simulation runs were conducted by changing the speed from 95 inches/min to 110 inches/ min to have better comparison. During the temperature measurements and for simulations, the water flow rate in the mould and secondary cooling zone were taken as constant and their effect on casting speed was not considered.

Also, in Figure 34, we can see considerable change in temperature at zone 1 (23’<cutting torch). This was due to the pouring of fresh liquid steel into the tundish, which is at a much higher temperature than the steel in the tundish. This change in metal temperature was difficult to consider in the simulation model, and increased the error during comparisons.

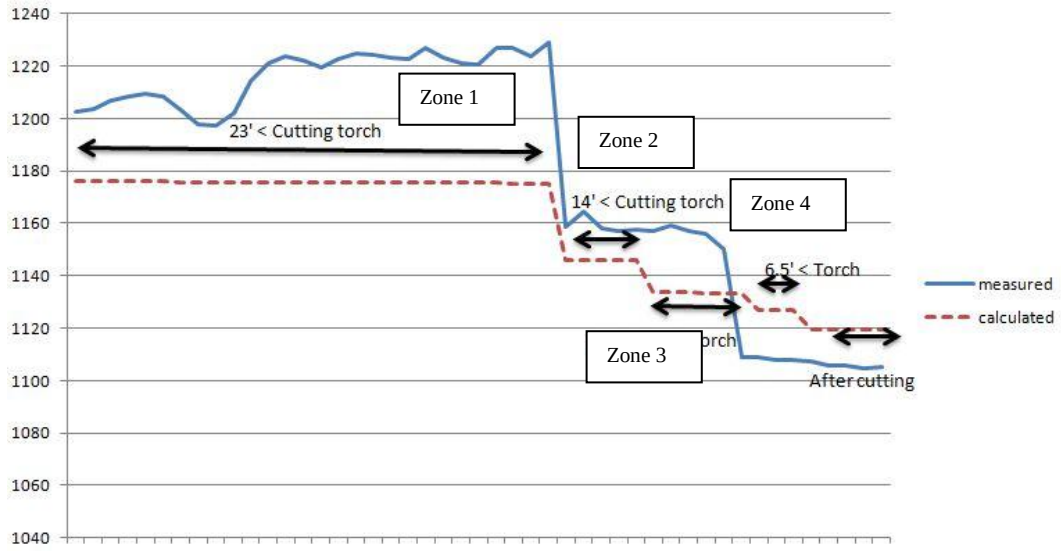

Figure 34: Measured versus calculated surface temperature for grade 1025 trial 2

5.2 Effect of Casting Speed:

Increasing the casting speed increases the mould heat transfer. Based on previous studies [57, 69] it was noticed that, due to shorter residence time of the steel billet at high casting speeds, a thinner shell was formed which reduced the gap between the mould and the billet letting out more heat from the surface[69]. It was also observed that the casting speed was the most important factor affecting thermal and solidification conditions[70]. Hence, it is very important to consider mould design parameters and water cooling rate before a substantial increase in casting speed.

Similarly, trials were taken for high carbon grade steel 5160 and Figures 35 and 36 demonstrate the comparison between measured and calculated data.

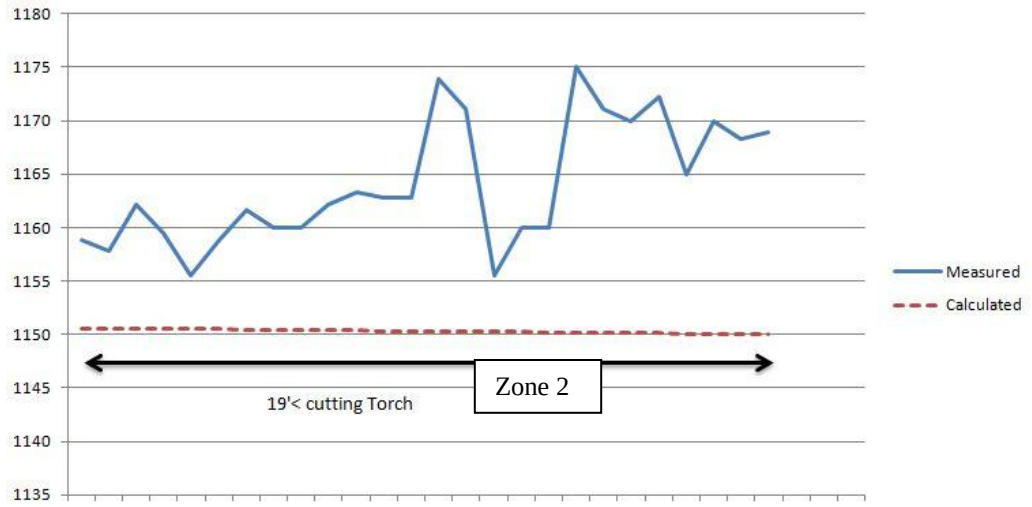

Figure 35: Measured versus calculated surface temperature for grade 5160 trial 1

Figure 35 demonstrates the effect of scaling on temperature measurement. Temperature measurement during this trial was taken at a casting speed of 106 to 108 inches /min. These fluctuation in temperature measurement occurred for very few trials and during the comparison maximum values were considered.

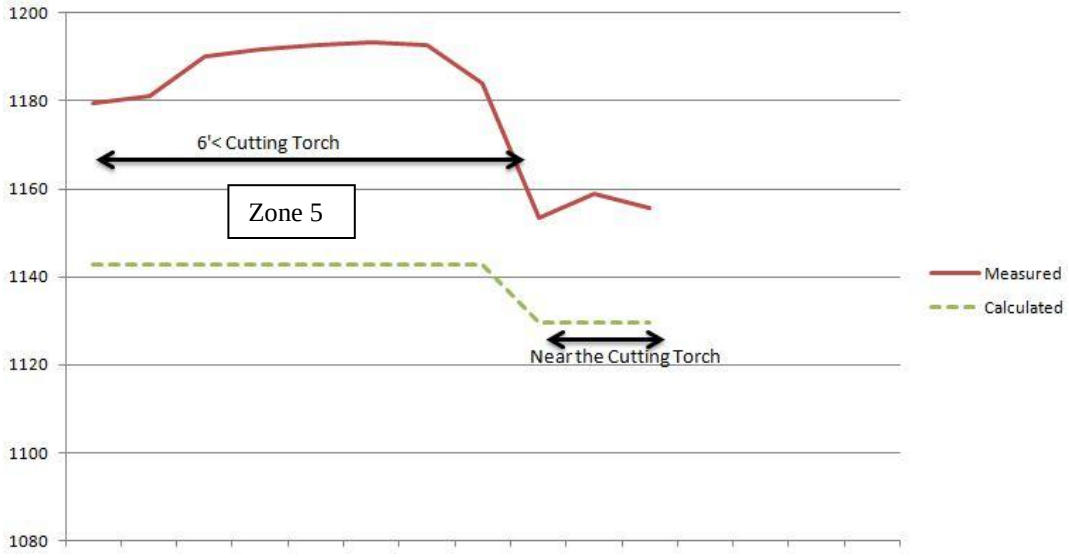

Figure 36: Measured and calculated surface temperature versus casting speed for grade 5160-2

In Figure 36 we can notice a small temperature increment due to variation in casting speed. This trial was taken at maximum casting speed at which Arcelormittal is currently

operated (130in/min). We can notice that very small variation in casting speed affects the temperature measurement considerably.

In some cases the calculated results are very low at zones where the measurements were taken. It is difficult to know where the error lies, either in measurement or calculation. The temperature measurement errors could be due to scale on the billet and may differ from calculated results due to the longer response time to the change in speed of the caster. It is known that the solidification and liquid pool depth changes with casting speed and the response time corresponds to the time required for the new condition to transmit at the new casting speed[58].

Possible errors between the calculated and measured temperatures were analyzed and were found to be reasonable. From Figures 33-36 the surface temperature predicted by the simulation model for grade 1025 (Figures 33 and 34) with defined boundary conditions agreed with the measured data within 3.5%-4.2%. For grade 5160 the error between the calculated and measured was between 2% to 4.2% (Figures 35 and 36). In a few cases it was noticed that calculated results varied a lot compared to the measured temperatures, e.g., near the gas cutting torch. This discrepancy between the two may be due to the possibility of delayed response time due to immediate change in casting speed[58]. The error in the software simulation was noted to be around 1.3%.

The surface temperatures measured at the curve near the straightener with an optical pyrometer for grades 1025 and 5160 are listed in Table 15.

Table 15: Measured versus calculated surface temperature for grades 1025 and 5160 at the curve section.

Grade 1025– Cast No.	**Measured**	**Calculated**	**Error**
M45402	1191	1160	2.6 %
M46067	1203	1176	2.2%
Grade 5160– Cast No.	**Measured**	**Calculated**	**Error**
M46965	1159	1150	0.7 %

It can be noticed from Table 15 that the calculated surface temperatures are reasonable with an error less than three percent and in most of the cases the accuracy of the system lays approximately within $\pm$ 30-40 ° C.

Figures 37 and 38 show two curves giving the center and surface temperature along the strand obtained through simulation at the maximum operated speed of 130 inches/min for grades 1025 and 5160 respectively.

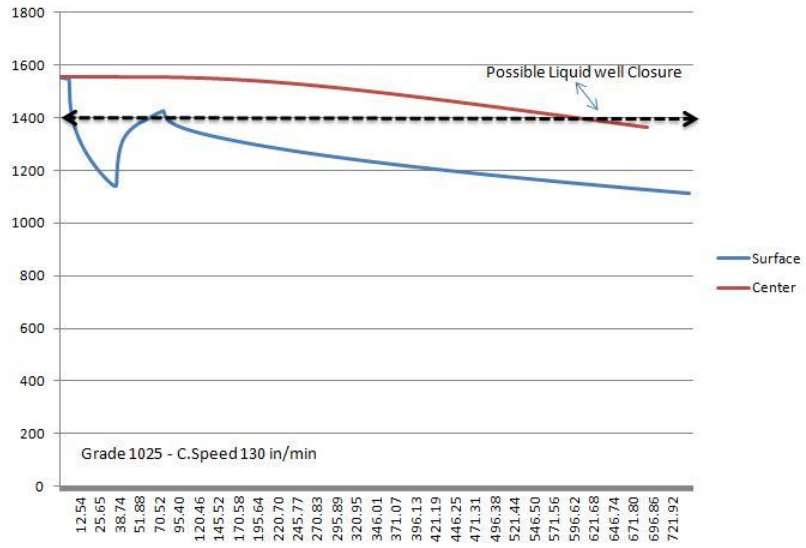

Figure 37: Temperature at the surface and center of the billet for grade 1025

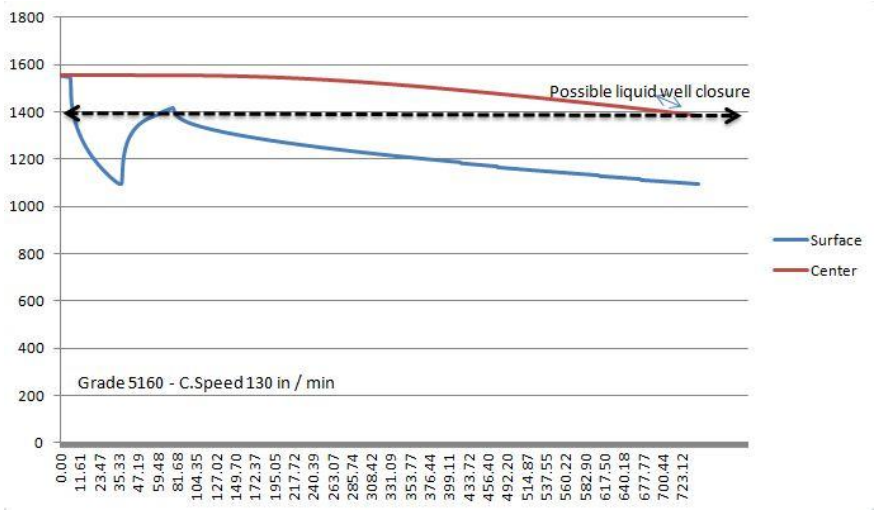

Figure 38: Temperature at the surface and center of the billet for grade 1025

Liquid well closure is the section where the solidifying billet is below the melting temperature and the center core is assumed to be completely solid below this temperature.

The center and surface temperature data acquired from the simulation can thus be utilized to determine a safe increase in casting speed. The liquid well closure can be predicted once the center temperature crosses the solidus value of the metal being cast. Center and surface temperature data were captured for different casting rates, i.e., 120, 130, 134 and for 140 inches/min (Tables 16 – 19). By comparing these data for the zone very near to the cutting torch, possibilities of increasing the casting speed were studied.

Table 16: Center and surface temperatures for grade 1025 and 5160 for the end section of one foot at a casting rate of 120 inches/min

Distance	**Temperature data for a casting speed 120 in/ min**			
Inches	**Grade 1025 Surface**	**Grade 1025 Center**	**Grade 5160 Surface**	**Grade 5160 Center**
0.00	1101	1343	1087	1373
1.26	1100	1342	1087	1372
2.45	1100	1342	1087	1372
3.65	1100	1341	1086	1371
4.84	1099	1341	1086	1371
5.44	1099	1340	1086	1370
6.63	1099	1340	1086	1370
7.82	1099	1339	1085	1369
8.42	1098	1339	1085	1369
9.61	1098	1338	1085	1369
10.81	1098	1338	1085	1368
11.40	1098	1337	1084	1368
12.00	1097	1337	1084	1368

Table 17: Center and surface temperatures for grade 1025 and 5160 for the end section of one foot at a casting rate of 130 inches/min

Distance	Temperature data for a casting speed 130 in/ min			
	Grade 1025	Grade 1025	Grade 5160	Grade 5160
Inches	Surface	Center	Surface	Center
0.00	1117	1369	1097	1387
1.26	1116	1369	1097	1387
2.45	1116	1368	1097	1386
3.65	1116	1368	1096	1386
4.84	1115	1367	1096	1385
5.44	1115	1367	1096	1385
6.63	1115	1366	1096	1384
7.82	1115	1366	1095	1384
8.42	1114	1366	1095	1383
9.61	1114	1365	1095	1383
10.81	1114	1365	1094	1382
11.40	1114	1364	1094	1382
12.00	1114	1364	1094	1382

Table 18: Center and surface temperatures for grade 1025 and 5160 for the end section of one foot at a casting rate of 134 inches/min

Distance	Temperature data for a casting speed 134 in/ min			
	Grade 1025	Grade 1025	Grade 5160	Grade 5160
Inches	Surface	Center	Surface	Center
0.00	1122	1378	1103	1397
1.26	1122	1378	1102	1397
2.45	1122	1377	1102	1396
3.65	1121	1377	1102	1396
4.84	1121	1376	1101	1395
5.44	1121	1376	1101	1395
6.63	1121	1375	1101	1394
7.82	1120	1375	1101	1394
8.42	1120	1375	1101	1394
9.61	1120	1374	1100	1393
10.81	1120	1374	1100	1393
11.40	1119	1374	1100	1392
12.00	1119	1373	1100	1392

Table 19: Center and surface temperatures for grade 1025 and 5160 for the end section of one foot at a casting rate of 140 inches/min

Distance	Temperature data for a casting speed 140 in/ min			
Inches	Grade 1025 Surface	Grade 1025 Center	Grade 5160 Surface	Grade 5160 Center
0.00	1130	1390	1110	1410
1.26	1130	1390	1110	1409
2.45	1130	1390	1110	1409
3.65	1129	1389	1109	1409
4.84	1129	1389	1109	1408
5.44	1129	1388	1109	1408
6.63	1129	1388	1109	1407
7.82	1128	1388	1108	1407
8.42	1128	1387	1108	1407
9.61	1128	1387	1108	1406
10.81	1128	1386	1108	1406
11.40	1128	1386	1108	1406
12.00	1127	1386	1107	1405

The results of the investigation clearly demonstrated that there was very little possibility of increasing the casting rate above 134 in/min as it may lead to cutting the billet with release of liquid steel.

The maximum casting rate that Arcelormittal has been using (130 in/min) is within the solidus temperature limit. The casting rate can be raised to 134 in/min without violating any of the casting constraints, which is well supported by observing the fraction of liquid phase plot (Figure 39) for the casting rate of 134 in/min.

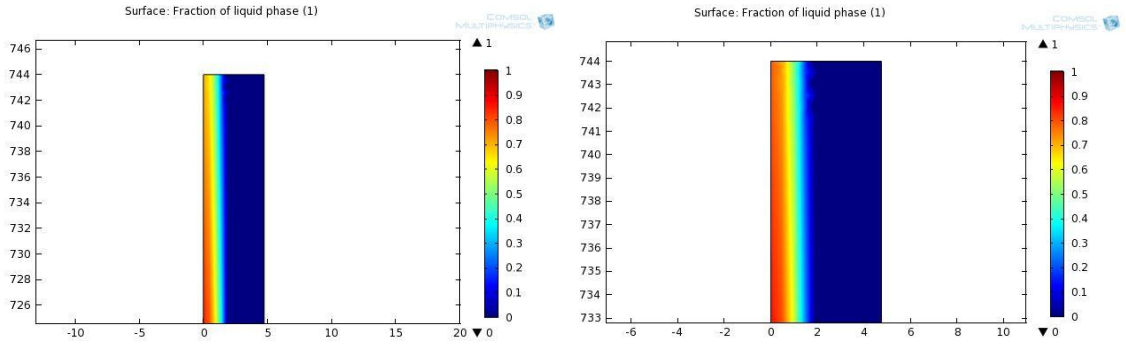

Figure 39: Fraction of liquid phase plot for grade 1025(left) and 5160 (right)

A three percent increase in casting speed can be implemented. However, continuous monitoring of the surface temperature with consideration of the errors between calculated and measured temperatures should be undertaken.

5.3 Discussion

The aim of the present work was to develop a heat transfer model which predicted the temperature distribution along the strand for a continuous casting machine, and therefore, to be able to determine the maximum possible speed for the caster under present cooling conditions. A 2D non-isothermal heat transfer stationary model was used along with pyrometer measurement of operating temperatures at Arcelormittal Contrecoeur West. The model predicted the temperature distribution as a function of steel inlet temperature, withdrawal speed, heat transfer coefficient, and phase change phenomenon. All comparisons between measured and predicted surface temperatures showed that the predictions were within $\pm$ 30-40 °C of the measurements, i.e., 2-4% error. In summary, the model gave reliable results.

Arcelormittal Contrecoeur West is in the process of implementing higher casting speeds by installing pyrometers along the strand to measure surface temperatures to be used as feedback signals to control the speed of the caster.

Chapter 6 : Conclusion and Future work

6.1 Conclusion

In this part of the study, a 2D stationary non-isothermal heat transfer model has been developed. The simulation model calculates the fraction of liquid phase and heat distribution along the strand length. The model was tested by comparing empirical data obtained through plant trials to simulation data, where good agreement between the calculated and measured results was achieved. The simulation and experimental techniques can be used to verify heat distribution along the length of the mould, and by knowing the effect of casting speed on temperature distribution, a possible gain in casting speed and improvements in casting quality can be obtained. A maximum speed for the casting operation at Arcelormittal Contrecoeur was found to be 134 in/min.

6.2 Future Considerations

As to possible future work, the main aim would be to study more precisely the heat transfer conditions in the mould and secondary cooling zones. By further extending the model development, an even better model could be created to control the process. In addition, a simulation of the model and pyrometer measurements could be used together to control the speed of the caster, the rate of mould cooling water, and the secondary water flow rate in real time to optimize the caster speed.

References

1. *Steel Industry*. 2012; Available from: http://bx.businessweek.com/steel-industry/news/.
2. D. Janke, L.S., H.J Weddige, E Schilz *Scrap based steel production and recycling of steel*. 2000.
3. *Alloying of steels*. 2012; Available from: http://materialsengineer.com/E-Alloying-Steels.htm.
4. *Crude steel production*. 2012; Available from: http://www.worldsteel.org/media-centre/press-releases.html.
5. *Steel production gas power*. 2011; Available from: http://www.clarke-energy.com/gas-type/steel-production-gas/.
6. *Arcelormittal fact book*. 2010.
7. *Arcelormittal Dofasco*. Available from: http://www.dofasco.ca/bins/content_page.asp?cid=339-9516-307970.
8. *Arc Furnace Digest*, 2001, The UCAR®.
9. J. Maiolo, V.S., P. Clerici *Dynamic process control for the Electric Arc Furnace*. AISTech, 2009. **1**.
10. *Slag atlas*1981, Du\0308sseldorf: Verlag Stahleisen M B H.
11. E.B Pretorius, R.C.C., *Foamy slag fundamentals and their practical application to electric furnace steelmaking*, 1999, Iron & Steel Society: Warrendale, PA, ETATS-UNIS.
12. Bul'ko B. , K.J., Domovec M. *Optimization Slag Composition In Ladle Furnace Considering To Effective Steel Desulfurization* 2009. 93-99.
13. R.J Fruehan, Y.L., and L.Barbie, *Dissolution of magnesite and Dolomite in Simulated EAF Slags*, in *ISS Tech Conference*April 2003. p. 799-812.
14. Bruce Kozac., J.D. *Continuous Casting of Steel: Basic Principles*. 2012; Available from: http://www.steel.org/en/Making%20Steel/How%20Its%20Made/Processes.aspx.
15. *EFSOP*. Available from: http://www.tenovagroup.com/efsop_systems.php?id_prodotto=13.

16. Pretorius, E., *Fundamentals of EAF and ladle slags and Ladle refining principles*, Baker Refractories. p. 73.
17. Kemeny, F.L., Sosinsky, D J. *Synthetic Ladle Slag Engineering for Improved Chemistry and Ladle Life*. in *48th Electric Furnace Conference Proceedings*. 11-14 Dec. 1990. New Orleans, Louisiana; USA.
18. Dictionaries, O., *"Slag"*April 2010: Oxford University Press.
19. Dippenaar, R., *Industrial uses of slag (the use and re-use of iron and steelmaking slags).* Ironmaking & steelmaking, 2005. **32**(1): p. 35.
20. *Steel Plant Training Course*. Available from: http://www.carmeusena.com/files/files/brochures/shopversionelectricfurnaceslagtrainingsection.pdf.
21. E. B. Pretorius, R.C.N. *Stainless steel slag fundamentals - from furnace to tundish*. 58th Electric Furnace Conference and 17th Process Technology Conference, 2000. **1**, 133.
22. *Electric Arc Furnace*. [cited 2012; Available from: http://www.substech.com/dokuwiki/doku.php?id=electric_arc_furnace_eaf.
23. *Basicity* Available from: http://encyclopedia2.thefreedictionary.com/Basicity.
24. Duffy, J.A. and M.D. Ingram, *Establishment of an optical scale for Lewis basicity in inorganic oxyacids, molten salts, and glasses.* Journal of the American Chemical Society, 1971. **93**(24): p. 6448-6454.
25. Duffy, J.A. and M.D. Ingram, *An interpretation of glass chemistry in terms of the optical basicity concept.* Journal of Non-Crystalline Solids, 1976. **21**(3): p. 373-410.
26. Ghosh, D., *Application of optical basicity to viscosity of high alumina blast furnace slags.* Journal of mining and metallurgy. Section: B, Metallurgy, 2010. **46**(1): p. 41-49.
27. Duffy, J.A., *Acid-base properties of molten oxides and metallurgical slags.* Journal of the Chemical Society. Faraday Transactions I, 1978. **74**: p. 1410-1419.
28. E. Burstrom, G., Ye, J. Von Scheele, and R. Selin, *Mechanism of Formation of Foamy Slags in Electric Arc Furnace*, in *4th International Conference on Molten Slags and Fluxes*1992, ISIJ: Sendai. p. 352-357.

29. Mills, K., *The estimation of slag properties*, 2011, Department of Materials, Imperial College, London, UK. p. 56.
30. Millman, M.S., *Secondary steelmaking developments in british steel*, 1999, Maney Publishing. p. 169-175.
31. Arc, The Columbia Encyclopedia (3rd ed.): New York.
32. Stephen, F.M., *Improvement of the desulfurization process by slag composition control in the ladle furnace.*, in *Minerals And Metallurgical Engineering*2009, Lulea University of technology. p. 66.
33. Oltmann, E.P.a.H., *Desulfurization*, LWB Refractories.
34. Margareta Andersson, P.G.J., Mselly M. Nzotta, *Application of Sulphide Capacity Concept on High basicity Ladle Slags Used in Bearing Steel Production*, in *ISIJ International, Vol 39*1999. p. pp 1140-1149.
35. Marr, E.P.a.R., *Computer modeling of refractory/slag/metal interactions*, in *International Conference on molten slag, fluxes and salts*1997: Australia.
36. James Bennett, R.K., Kyei-Sing Kwong, Arthur Petty & Hugh Thomas, *Thermodynamic studies of MgO saturated EAF slag.* Ironmaking & steelmaking, 2010. **37**(7): p. 529.
37. *Factsage*. Available from: http://gtt.mch.rwth-aachen.de/gtt-web/factsage.
38. Jasper Kwong, J.P.B., Rick Krabbe *A computer model of MgO saturated EAF slag chemistry*.
39. *Degradation of MgO Refractory in CaO-SiO^sub 2^-MgO-FeO^sub x^ and CaO-SiO^sub 2^-Al^sub 2^O^sub 3^-MgO-FeO^sub x^ Slags Under Forced Convection.* Metallurgical and Materials Transactions; B; Process Metallurgy and Materials Processing Science, 2005. **36B**(4): p. 453.
40. Rait, *Basic refractories*1950, New York: Interscience publisher
41. H. G. Asth1, L.F.S., G. J. Cruz3, G. Bastos4 , L. P. Almeida5, R. S. Sampaio6 *Increasing the Refractory Wear Profile Control on the Steel Ladles at the V&M do Brazil*. 2010.
42. Pretorius, E.; Available from: http://etech.lwbref.com/Home/home.aspx.
43. *Stahl in Zahlen*. Available from: http://www.stahl-online.de/english/linke_Navigation/Steel_in_Figures/index.php.

44. Lait, J.E., *Solidification and heat transfer in the continuous casting of steel*, in *Metallurgy*1973, The University of British Columbia: Vancouver. p. 142.
45. Louhenkilpi, S., *Real-time simulation of heat transfer in continuous casting.* Metallurgical transactions. B, Process metallurgy, 1993. **24**(4): p. 685.
46. Yu, K.O., *Modeling for casting and solidification processing*2002, New York: Marcel Dekker, Inc.
47. Tieu, A.K. and I.S. Kim, *Simulation of the continuous casting process by a mathematical model.* International Journal of Mechanical Sciences, 1997. **39**(2): p. 185-192.
48. Sowa, L. and A. Bokota, *Numerical Model of Thermal and Flow Phenomena the Process Growing of the CC Slab*, 2011. p. 359.
49. Fic, A., A.J. Nowak, and R. Bialecki, *Heat transfer analysis of the continuous casting process by the front tracking BEM.* Engineering Analysis with Boundary Elements, 2000. **24**(3): p. 215-223.
50. Chow, C. and I.V. Samarasekera, *High speed continuous casting of steel billets: Part 1: General overview.* Ironmaking & steelmaking, 2002. **29**(1): p. 53-60.
51. Mäkinen, M. and M. Uoti, *Mould Temperature Fields during Continuous Casting of DHP-Copper*, in *Continuous Casting*2006, Wiley-VCH Verlag GmbH & Co. KGaA. p. 234-239.
52. Muojekwu, C., I. Samarasekera, and J. Brimacombe, *Heat transfer and microstructure during the early stages of metal solidification.* Metallurgical and Materials Transactions B, 1995. **26**(2): p. 361-382.
53. Raudensky, J.H.a.M. *Measurement of Heat Transfer Charecteristics of Secondary Cooling In Continuous Casting*. 2005.
54. Kee-Hyeon Cho, B.-M.K., *Numerical Analysis of Secondary Cooling in Continuous Slab Casting.* J. Mater. Sci. Technol., 2008. **24**(03): p. 389-390.
55. Pehlke, R.D. *Computer Simulation of Solidification Processes - The Evolution of a Technology*. 2001.
56. Kung, E.Y., *A mathematical model of heat transfer in continuous casting.* Simulation, 1968. **10**(1): p. 29.

57. Grill, A., K. Sorimachi, and J. Brimacombe, *Heat flow, gap formation and break-outs in the continuous casting of steel slabs.* Metallurgical and Materials Transactions B, 1976. **7**(2): p. 177-189.
58. Richard A. Hardin, K.L.a.C.B. *Development of A Model For Transient Simulation And Control of a continuous Steel Slab Caster*.
59. Spalding, D.B. *A guide to the PHOENICS input language - CHAM TR/100*. 1993.
60. Sismanis, P., *Modeling Solidification Phenomena in the Continuous Casting of Carbon Steels, Two Phase Flow, Phase Change and Numerical Modeling, Amimul Ahsan (Ed.),* InTech: Greece.
61. Ying Li, Y.Z., Haicheng Xu,Zhiguang Ao, *Computer simulation of solidification heat transfer in continuous casting bloom*, 2010, WRI Global Congress on Intelligent Systems. p. 9-12.
62. Louhenkilpi, S., E. Laitinen, and R. Nieminen, *Real-time simulation of heat transfer in continuous casting.* Metallurgical and Materials Transactions B, 1993. **24**(4): p. 685-693.
63. Fjellstedt, J. and A.E.W. Jarfors, *On the precipitation of TiB2 in aluminum melts from the reaction with KBF4 and K2TiF6.* Materials Science & Engineering, 2005. **413-414**: p. 527-532.
64. COMSOL Multiphysics User's Guide, V. 2011.
65. *The Engineering Tool Box*. Available from: http://www.engineeringtoolbox.com/overall-heat-transfer-coefficient-d_434.html.
66. *efunda*. Available from: http://www.efunda.com/materials/alloys/alloy_home/search_alloy.cfm.
67. *Newport*. Available from: http://www.newportus.com/Products/Techncal/MetlEmty.htm.
68. *Special Steel Suppliers*. Available from: http://www.steelss.com/Carbon-steel/aisi-5160.html.
69. Guo, L., *Mould heat transfer in the continuous casting of round billet.* ISIJ International, 2007. **47**(8): p. 1108.
70. R.A. Hardin, K.L.a.C.B. *Development of the model for transient simulation and control of a continuous steel slab caster*2000. **3**, 61-74.